International Journal of Non–Linear Mechanics 165 (2024) 104816

Contents lists available at ScienceDirect

International Journal of Non-Linear Mechanics

journal homepage: www.elsevier.com/locate/nlm

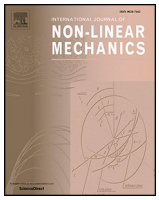

# Nonlinear dynamic response of the vibro-impact systems subjected to harmonic ground motion under conditions of uncertainty on the gap size

Domenico Pagano, Giuseppe Perna, Maurizio De Angelis *, Ugo Andreaus

*Sapienza University of Rome, Dipartimento di Ingegneria Strutturale e Geotecnica, Via Eudossiana, 18-00184, Roma, Italy*

ARTICLE INFO

*Keywords:*
Vibro-impact systems
Nonlinear dynamic response
Harmonic ground motion
Uncertainty on the gap size
Confidence zones
Probability distribution functions (PDFs)

ABSTRACT

In isolated structures, the large relative displacements with respect to the base that occur as a result of significant seismic actions can excessively deform and damage the isolation system or can lead to pounding with adjacent structures if the distance between the structures (gap) is not sufficiently large; this can result in local or structural damage and damage to equipment contained in the structure due to increased absolute accelerations. One way to mitigate this damage is to insert appropriate deformable and dissipative devices (bumpers) between adjacent structures. The objective of the work is to evaluate, by numerical analysis, how uncertainties on the gap parameter, initially assumed to be symmetrical and positive, can give rise to nonsymmetrical and negative gaps and can also significantly influence the nonlinear dynamic response of a vibro-impact single-degree-of-freedom system optimally designed and excited with harmonic excitation at the base. The main results obtained showed how the presence of an uncertainty in the gap, modeled through normal probability distributions, is reflected i) on the nonlinear dynamic response of the system with values that lie in frequency-dependent confidence zones, (ii) on the probability distributions of the response quantities (the absolute accelerations and relative displacements of the mass and the deformations and forces in the bumpers), (iii) on the width of the intervals in which the probability distributions of the response turns out to be of normal distributions, (iv) on the link between the gap values and the values obtained from the different response quantities considered.

## 1. Introduction

Base isolation system represents one of the most widely applied passive control strategies to mitigate the dynamic response of structures and equipment [1]. In contrast, semi-active isolation systems, using sensors, processors and actuators, allow the mechanical parameters (such as stiffness [2]) of control devices to be adjusted in real time so limiting problems due to large displacements. The objective of base isolation is to decouple the movement of the structure from that of the ground by introducing a highly horizontally deformable element (the isolator) between the substructure and the structure, so as to significantly increase the period of oscillation of the system and reduce the absolute acceleration transmitted to the structure.

Thus, this control strategy is characterized by isolation devices that have a low stiffness value; this can produce large horizontal relative displacements concentrated in the isolation system under both static and dynamic actions such as Near Fault (NF) earthquakes, which are characterized by pulses with a long period and high intensity [3–5]. Large displacements on the one hand can severely damage isolation devices by exceeding their deformation limit (leading them to permanent deformation or rupture), and on the other hand can lead to pounding with adjacent retaining walls or adjacent structures [6–9] if the available gap is not large enough. Potential pounding can lead to consequences ranging from minor local structural damage to severe structural damage or even collapse of structures [10–12]; in fact, pounding generates increases in both accelerations and interstorey drifts in isolated structures. High increases in accelerations are strongly influenced by the stiffness of the impacting elements (hard impact) and, at the floors where impact occurs, affect the floor response spectra with possible damage to any vulnerable equipment [10]. Increases in interstorey drifts, on the other hand, can lead to permanent deformations or failure of structural and nonstructural elements.

One possible way to reduce excessive displacements is to add Tuned Mass Dumper systems (TMD) equipped with Inerter to traditional base isolation systems [13–16]. The Inerter is a two-terminal device, proposed by Smith [17], able to develop a resisting force proportional to the

* Corresponding author.
*E-mail addresses:* domenico.pagano@uniroma1.it (D. Pagano), giuseppe.perna@uniroma1.it (G. Perna), maurizio.deangelis@uniroma1.it (M. De Angelis), ugo.andreaus@uniroma1.it (U. Andreaus).

https://doi.org/10.1016/j.ijnonlinmec.2024.104816
Received 7 March 2024; Received in revised form 22 May 2024; Accepted 23 May 2024
Available online 28 June 2024

relative acceleration of its ends by a constant called "inertance". The performance of these new systems, referred to in the literature as Tuned Mass Damper Inerter (TMDI), has been extensively studied and demonstrated both numerically [13–16,18,19] and experimentally [20–22].

Another possible mitigation method to prevent damage to the isolation system due to pounding is the interposition of deformable and dissipative (soft impact) devices (bumpers) placed at a certain distance (gap) [12,23], which on the one hand limit the displacement of the structure and on the other hand reduce (if properly designed) the increases in accelerations that occur as a result of pounding. The dynamic response of these new isolation systems equipped with bumpers, named Vibro-Impact Isolation Systems (V-IIS), can be very varied: primary and secondary resonances, left and right hysteresis, irregular resonances, quasi-chaotic and chaotic responses [24–32].

V-IISs subjected to harmonic excitation at the base have been extensively studied by the authors of this article [32–40], from these studies it was found that the parameters affecting the nonlinear dynamic response are, in addition to frequency, the gap (distance between the mass and the bumpers), stiffness and damping of the bumpers. The authors also showed how the non-smooth dynamic response that characterizes V-IISs can be made smooth by designing the bumpers by imposing an optimality relationship [32,41] between the stiffness and damping of the bumpers and the damping coefficient of the isolator (damper), and the optimality curve [41,42] that links the value of the gap to the value of the stiffness of the bumpers, reducing the optimal design to the gap parameter only.

As shown in Ref. [43] the uncertainties come principally from two different factors: 1) the first uncertainty factor comes from the imperfections and idealizations made in the formulation of the physical models, as well as from the choices made on the types of probability distributions for representing the uncertainties; these uncertainties are called *model uncertainties*; 2) the second uncertainty factor comes from parameters such as geometry, material properties, actions, boundary and initial conditions, etc.; these uncertainties are called *data uncertainties*. One way to handle the inevitable uncertainties governing a problem is to use probabilistic criteria and analysis.

Structures are frequently subject to stochastic time-dependent actions, such as natural phenomena from wind gusts, earthquakes, random noise, etc. The influence that stochastic actions have on the dynamic response of single-degree-of-freedom vibro-impact systems has attracted the attention of many researchers, who have developed various analysis methods, such as Markov processes method, stochastic averaging method, mean impact Poincaré map method [44–50], to obtain the system response under such actions. The research conducted shows how the nature of the stochastic action is reflected in the response quantities of the system, which also exhibit a stochastic character and are typically represented by their probability distribution functions, histogram plots, Poincaré maps and limit cycles.

In [43] a vibro-impact system (Timoshenko beam with an elastic barrier) is treated in which two different types of uncertainties, modeled through a gamma probability distribution, are considered, the former on the parameters of the Timoshenko beam (mass, stiffness and damping) and the latter on the stiffness of the elastic barrier; through the use of confidence zones it is shown how these uncertainties affect the nonlinear dynamic response of the system.

In [51–53] a possible method for governing uncertainties through controlled synchronization is shown; specifically, a slave system follows the response of a master system by applying to the slave system, through an actuator, an additional forcer with a defined control law so as to compensate for any parameter uncertainties.

The uncertainties considered in this work are related exclusively to the only design parameter of the V-IIS, namely the gap. The uncertainties involved in the values of the gaps of the two bumpers come principally from errors in the positioning of the bumpers or from accidental position changes that may occur later, as was observed in one of the experimental campaigns carried out by some of the authors of this paper [40]. To account for the influence of gap uncertainties on the nonlinear dynamic response, a normal probability distribution was used.

The objectives of this work are.

- to study the influence of gap uncertainties (excursion and eccentricity) on the nonlinear dynamic response of single-degree-of-freedom vibro-impacting systems designed through the optimality relationship and optimality curve;
- statistically evaluate the nonlinear dynamic response (absolute acceleration and relative displacement of mass, deformation and force in bumpers) in terms of excursion and eccentricity;
- evaluate the relationship connecting the uncertainties (excursion and eccentricity) of the gaps to the excursion and eccentricity of the nonlinear dynamic response;
- to characterize, through statistical tests, the probability distribution functions (PDFs) of the nonlinear dynamic response in terms of excursion and eccentricity;

The paper is organized as follow Section 2 presents the numerical model and the equations of motion; Section 3 shows the results necessary to understand both the nonlinear dynamic response of V-IIS and the possible scenarios; Section 4 defines the bumpers configurations in a pseudo-random way and shows the system response through confidence zones; Section 5 shows how the response quantities are distributed and identifies the normality preservation intervals; finally, the main conclusions and future developments are given in Section 6.

## 2. Equation of motions

The study was conducted considering a single degree of freedom (SDOF) vibro-impacting system (shown in Fig. 1), composed of a mass $M$ (highlighted in green), a damper $D$ (highlighted in blue) and two deformable and dissipative bumpers (highlighted in red) indicated, respectively, as right bumper ($B_R$) and left bumper ($B_L$), i.e. $B_j$ with $j = R,L$. The bumpers are positioned on both sides of the mass at an initial distance (initial gap) $G_{0j}$ ($j = R, L$). The damper and bumpers are modeled using a linear elastic element with stiffness $K$ and $K_j$ ($j = R,L$), respectively, and a linear viscous damper with damping coefficient $C$ and $C_j$ ($j = R,L$), respectively; these elements are arranged in parallel as shown in Fig. 1.

The system is subject to a harmonic base acceleration $A_t(t) = A_G \sin \Omega t$, characterized by an amplitude $A_G$ and circular frequency $\Omega$. The relative displacements of the mass with respect to the ground and the deformations of the bumpers are indicated, respectively, as $u$ and $u_j$ ($j = R,L$).

The equations of motion are written in dimensionless form to make

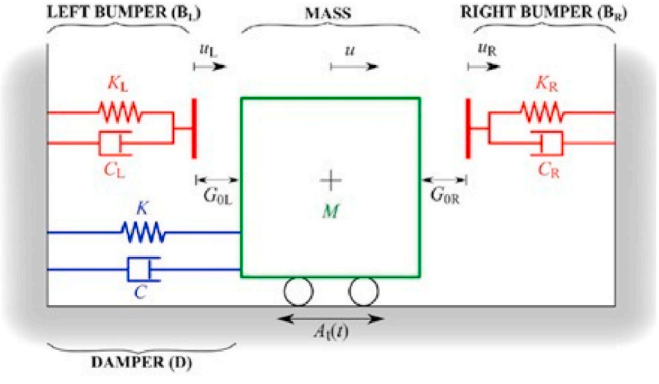


**Fig. 1.** Model of the SDOF system with the two lateral bumpers: the mass of the system is highlighted in green, the damper is represented in blue, while the right and left bumpers are represented in red.

them as general as possible. The components of the equation are normalized with respect to the term $F^* = M\omega^2 u^*$, which represents the maximum force in the SDOF system in free flight (without impact, FF): the quantity $u^* = u_{st} R_{d,max}$ represents the maximum relative displacement in FF, where $u_{st} = A_G/\omega^2$ is the static displacement and $R_{d,max} = 1/\left(2\xi\sqrt{1-\xi^2}\right)$ is the maximum value of the dynamic amplification in displacement (i.e. the value of the dynamic amplification factor in displacement $R_d(\xi,\beta)$ evaluated for the value of $\beta$ for which the resonance in displacement occurs), finally $\omega = \sqrt{K/M}$ is the natural frequency of the system.

To write the dimensionless equations in compact form, the following dimensionless quantities are defined: the dimensionless time $\tau = \omega t$, the dimensionless relative displacement of the mass $q = u/u^*$ and the dimensionless deformation of the bumpers $q_j = u_j/u^*$ ($j = R, L$), the damping ratio of the SDOF system $\xi = C/(2M\omega)$, the maximum dimensionless of base excitation $a_G = 2\xi\sqrt{1-\xi^2}$, the frequency ratio $\beta = \Omega/\omega$ and the dimensionless gap $\delta_{0j} = G_{0j}/u^*$ ($j = R, L$). From the normalization adopted we have that the mass impacts the $j$-th bumper for $0 \le \delta_{0j} < 1$, while the mass is in free flight conditions if $\delta_{0j} \ge 1$. The force $f(\tau) = 2\xi q'(\tau) + q(\tau)$ is the dimensionless force of the damper; while $f_j(\tau) = 2\xi\gamma_j q'(\tau) + \lambda_j q_j(\tau)$ ($j = R, L$) are the dimensionless contact forces, where $\gamma_j = C_j/C$ and $\lambda_j = K_j/K$ are the dimensionless damping and stiffness of the bumpers. Finally, $a(\tau) = q''(\tau) + a_t(\tau)$ is the dimensionless absolute acceleration of the mass, where $a_t(\tau) = a_G \sin\beta\tau$ is the dimensionless harmonic acceleration at the base.

By dividing the equations of motion by the term $F^*$ and substituting the dimensionless quantities just introduced, the dimensionless equations can be written in the following form:

$$\begin{cases} q''(\tau) + 2\xi q'(\tau) + q(\tau) + f_j(\tau) \bullet \psi_1\left[\delta_j(\tau)\right] \bullet \psi_2\left[f_j(\tau)\right] = -a_G \sin\beta\tau & (1a) \\ f_i(\tau) = 0 & (1b) \end{cases} \tag{1}$$

where it is assumed that if $j = L$ in Eq. (1a), then $i = R$ in Eq. (1b), or if $j = R$ in Eq. (1a), then $i = L$ in Eq. (1b). In other words, Eq. (1a) governs the motion of the mass in contact with the $j$-th bumper, while Eq. (1b) refers to the free evolution of the $i$-th bumper; therefore, if the mass is in contact with the right bumper we will have $j = R$ and $i = L$, vice versa if the mass is in contact with the left bumper we will have $j = L$ and $i = R$.

The superscript ($'$) denotes the differentiation of the generic function made with respect to the dimensionless time $\tau$, while the Heaviside functions $\psi_k$ ($k = 1, 2$) are defined in the following way:

$$\textit{Contact} \quad \psi_1\left[\delta_j(\tau)\right] = \begin{cases} 0, \delta_j(\tau) > 0 \\ 1, \delta_j(\tau) = 0 \end{cases} \tag{2a}$$

$$\textit{Separation} \quad \psi_2\left[f_j(\tau)\right] = \begin{cases} 0, f_R(\tau) \le 0 \ \ or \ \ f_L(\tau) \ge 0 \\ 1, f_R(\tau) > 0 \ \ or \ \ f_L(\tau) < 0 \end{cases} \tag{2b}$$

where $\delta_j(\tau) = \delta_{0j} + \Delta q_j(\tau)$ ($j = R, L$), $\Delta q_R(\tau) = q_R(\tau) - q(\tau)$ and $\Delta q_L(\tau) = q(\tau) - q_L(\tau)$ is the clearance function and represents the distance, at any instant of time, between the mass and the $j$-th bumper. When the mass is in contact with the $j$-th bumper $\delta_j(\tau) = 0$, otherwise $\delta_j(\tau) > 0$.

Despite the relative simplicity of the model, in which both the damper and the bumpers were modeled using the Kelvin–Voigt model, the system is highly non-linear, due to the presence of the gaps, of the unilateral constraints and of the occurrence of the impact which causes abrupt changes in stiffness and damping upon contact.

As regards the beginning of the contact phase between the mass and the $j$-th bumper, it was identified based on the value of the clearance function $\delta_j(\tau)$ ($j = R, L$), as illustrated in Eq. (2a); the impact occurs when $\delta_j(\tau) = 0$. On the other hand, the evaluation of the time instant of the detachment is obtained based on the value of the contact force $f_j(\tau)$ ($j = R, L$), as illustrated in Eq. (2b). This condition is motivated by the need to overcome one of the drawbacks that the Kelvin-Voigt model has when it is used to model contact, i.e. the existence of attractive forces after the restitution phase; therefore, the change in sign of the contact force is assumed as a condition of separation between the mass and the bumper.

## 3. Nonlinear dynamic response of vibro-impacting systems

In this section the physical meaning of the response quantities is shown, what it means to have negative gap values, and through a series of comparisons it is evaluated how the dynamic response of the system changes as the excursion and eccentricity of the gap vary. In section 2 the initial configuration of the bumpers is uniquely identified through the initial dimensionless gaps $\delta_{0j}$ ($j = R, L$). However, the initial configuration of the bumpers can also be identified in terms of the initial excursion $\delta_0$ of the dimensionless gap, defined as the sum of the dimensionless initial gaps, and in terms of the initial eccentricity $e_0$ of the dimensionless gap, defined as the difference between the two dimensionless initial gaps.

These two ways of representing the initial configuration of the bumpers are linked through the following relations:

$$\begin{cases} \delta_0 = \delta_{0R} + \delta_{0L} & (3a) \\ e_0 = \delta_{0R} - \delta_{0L} & (3b) \end{cases} \tag{3}$$

$$\begin{cases} \delta_{0R} = (\delta_0 + e_0)/2 & (4a) \\ \delta_{0L} = (\delta_0 - e_0)/2 & (4b) \end{cases} \tag{4}$$

Since in this study the initial configuration of the bumpers is not assumed exclusively symmetrical, it is considered appropriate to describe this configuration in terms of $\delta_0$ and $e_0$.

In this section, various comparisons are carried out among different initial configurations of the bumpers; in these comparisons the mechanical parameters of the bumpers $\lambda_j$ and $\gamma_j$ ($j = R, L$) remain always the same. The dimensionless stiffness $\lambda_j$ and the dimensionless damping $\gamma_j$ are obtained by an optimal design in an initial reference configuration of the bumpers. In the results shown below, a value of $\delta_0 = 0.06$ and a value of $e_0 = 0$ are assumed for the reference configuration; therefore, for the reference configuration the two gaps are assumed to be symmetrical and with zero eccentricity. Once the reference configuration of the bumpers is known, it is possible to obtain the dimensionless stiffness $\lambda_R = \lambda_L = \lambda$ by entering the optimality curve with a value of $\delta = \delta_0/2$; once the value of $\lambda$ is known, the value of $\gamma_R = \gamma_L = \gamma$ is calculated via the optimality relation.

### 3.1. Physical meaning of the response quantities

When the system is subject to actions of a harmonic nature, the most effective way to describe the response of the system is through Pseudo-Resonance Curves (PRCs), i.e. analyzing the response of the system in the frequency domain; this way of viewing the response allows us to show how the system behaves in steady state conditions for each value of the dimensionless frequency of the forcing $\beta$.

In Section 4, Pseudo-Resonance Curves are used to illustrate the response of the system. The PRCs are plotted for response quantities which allow particular behaviors of the system to be highlighted; it is therefore necessary to define these response quantities.

Fig. 2 shows four response quantities considered fundamental to describe the behavior of a vibro-impacting system: relative displacement (a) and absolute acceleration of the mass (b), deformations (c) and contact forces (d) of the bumpers. The response quantities, of which the PRCs are reported in Section 4, are obtained -for each value of the dimensionless frequency of the forcing-starting from the time histories shown in Fig. 2.

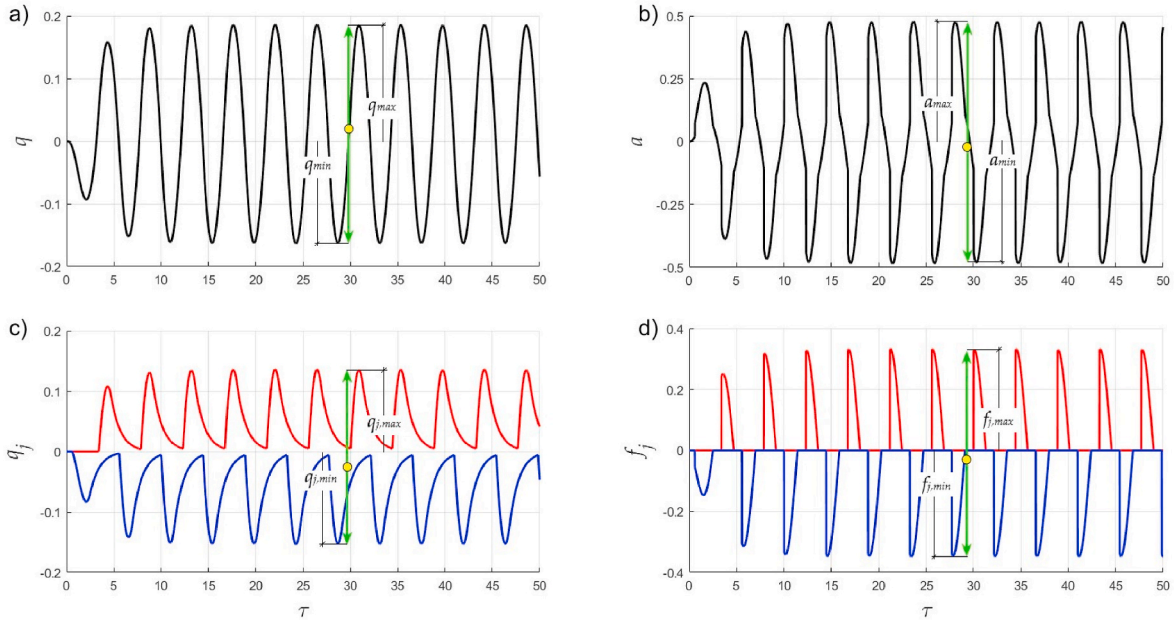


**Fig. 2.** Time histories of the selected response quantities obtained for a value of $\xi = 0.1$, for $\beta = 1.42$ (acceleration resonance frequency of the reference configuration), for values of $\lambda = 1.14$ and $\gamma = 5.70$ which derive from the optimal design relating to the reference configuration ($\delta_0 = 0.06$, $e_0 = 0$) and for $\delta_0 = 0.06$ and $e_0 = 0.04$; in a) and b) the time histories of the relative displacement and absolute acceleration of the mass are reported respectively, while in c) and d) the time histories of the deformations and contact forces of the bumpers are reported respectively. The double green arrow and the yellow dots represent, respectively, the excursion and eccentricity of the generic response quantity.

$$\begin{cases} \eta_{d,exc} = \dfrac{q_{max} - q_{min}}{q^0_{max} - q^0_{min}} \ (excursion\ of\ the\ relative\ displacement\ of\ the\ mass) & (5a) \\ \eta_{d,ecc} = \dfrac{q_{max} + q_{min}}{q^0_{max} - q^0_{min}} \ (eccentricity\ of\ the\ relative\ displacement\ of\ the\ mass) & (5b) \end{cases} \tag{5}$$

$$\begin{cases} \eta_{a,exc} = \dfrac{a_{max} - a_{min}}{a^0_{max} - a^0_{min}} \ (excursion\ of\ the\ absolute\ acceleration\ of\ the\ mass) & (6a) \\ \eta_{a,ecc} = \dfrac{a_{max} + a_{min}}{a^0_{max} - a^0_{min}} \ (eccentricity\ of\ the\ absolute\ acceleration\ of\ the\ mass) & (6b) \end{cases} \tag{6}$$

$$\begin{cases} \eta_{B,exc} = \dfrac{q_{j,max} - q_{j,min}}{q^0_{max} - q^0_{min}} \ (excursion\ of\ the\ deformations\ of\ the\ bumpers) & (7a) \\ \eta_{B,ecc} = \dfrac{q_{j,max} + q_{j,min}}{q^0_{max} - q^0_{min}} \ (eccentricity\ of\ the\ deformations\ of\ the\ bumpers) & (7b) \end{cases} \tag{7}$$

$$\begin{cases} \eta_{F,exc} = \dfrac{f_{j,max} - f_{j,min}}{f^0_{max} - f^0_{min}} \ (excursion\ of\ the\ contact\ forces\ of\ the\ bumpers) & (8a) \\ \eta_{F,ecc} = \dfrac{f_{j,max} - f_{j,min}}{f^0_{max} - f^0_{min}} \ (eccentricity\ of\ the\ contact\ forces\ of\ the\ bumpers) & (8b) \end{cases} \tag{8}$$

In Eqs. (7) and (8) the index $j$ takes on the values $R$ and $L$ (right bumper and left bumper).

As can be seen from the relationships reported in Eqs. (5)–(8), each of the response quantities reported in Fig. 2 is associated with two other response quantities, i.e. the maximum excursion and the eccentricity of the response quantity. In equations (5)–(8) reported above, the response quantities that appear on the right side are the maximum and minimum values that the generic response quantity attains in steady state conditions. Observing the numerator of Eq. (5a) it is possible to notice that this quantity is graphed in Fig. 2a with the double green arrow, whereas the numerator of Eq. (5b) is graphed in Fig. 2a with the yellow dot; similarly the numerator of Eqs. (6)–(8) is reported, respectively, in Fig. 2b,c,d.

The response quantities just illustrated (represented with the double green arrow and the yellow dot in Fig. 2) are also normalized by appropriate quantities; the normalization is done with respect to the response quantities that occur in resonance conditions for the system in free flight conditions. Each of the response quantities has its own value of $\beta$ for which resonance occurs and therefore there are time histories similar to those shown in Fig. 2 also for the FF condition: the response quantities reported in Eqs. (5) and (7) are divided by the excursion of the relative displacement of the mass in FF, the response quantities reported in Eq. (6) are divided by the excursion of the absolute acceleration of the mass in FF, finally, the response quantities reported in Eq. (8) are divided by the damper force excursion in FF.

The time histories shown in Fig. 2 were obtained for bumpers that have an eccentricity $e_0$ different from zero and, as can be seen from this figure, this leads to having response quantities that also have an eccentricity different from zero. In particular, passing from the notation $\delta_0$ and $e_0$ to that with $\delta_{0R}$ and $\delta_{0L}$ through the relations reported in Eq. (4), values of the left and right dimensionless gaps of: $\delta_{0R} = 0.05$ and $\delta_{0L} = 0.01$ are obtained. From the time history of the relative displacement of the mass, reported in Fig. 2a, it is possible to observe the presence of a positive eccentricity value of this response quantity; therefore the mass has greater relative displacements to the right, i.e. in correspondence with the largest gap. Vice versa, for the other three response quantities reported in Fig. 2 negative eccentricities of the response quantities are noted; therefore the absolute accelerations of the mass, the deformation and the contact force of the left bumper, i.e. the bumper which presents a smaller gap value, are slightly larger. The response of the system for bumpers with a positive eccentricity of the gap ($e_0 > 0$) can vary depending on the gap excursion and on the value of the forcing frequency, as will be shown in Sect. 4; therefore the time histories shown in Fig. 2 are representative of a particular configuration of the bumpers and of a particular value of the forcing frequency.

### 3.2. Physical meaning of the negative gaps

In the analyzes reported in Sect. 4, initial configurations of the bumpers $\delta_0$ and $e_0$ to which negative $\delta_{0R}$ and $\delta_{0L}$ values are associated will also be considered. It therefore becomes necessary to show what the physical significance of negative gap values is.

Fig. 3 shows an exhaustive list of the possible scenarios that can occur due to the pseudo-random generation of $\delta_0$ and $e_0$. From this figure it is possible to see how, for all four scenarios shown, configuration 0 (represented through the dotted lines in Fig. 3) is physically impossible, as it would give rise to an unbalanced initial configuration characterized by the interpenetration of the bumpers and of the mass. The negative gap values give rise to forces applied to the mass through the pre-compression of the bumpers, since if they could the bumpers would move to the 0 configuration, but since this configuration is not physically possible the system moves to an equilibrium and physically possible configuration, i.e. configuration 1 (or initial configuration of the bumpers).

The transition from configuration 0 to configuration 1 is thought to occur in static conditions and since it is not possible to know a priori whether a bumper is pre-stressed or not, (see cases c) and d)), this transition is carried out by solving a non-linear static problem, in which the non-linearity is inherent in the fact that it is not possible to know a priori whether the generic bumper will have to be inserted into the equilibrium equation or not. The static equilibrium equation at the initial instant changes based on the value assumed by the relative displacement of the mass and on the moment in which this displacement is obtained by solving the static equilibrium equation; therefore, it is necessary to proceed iteratively.

$$\begin{cases} q(0)+\lambda(q(0)-\delta_{R0})+\lambda(q(0)+\delta_{L0})=0 \quad if \;\; \delta_R=\delta_L=0 \quad (9a) \\ q(0)+\lambda(q(0)-\delta_{R0})=0 \quad if \;\; \delta_R=0 \; e \; \delta_L>0 \quad (9b) \\ q(0)+\lambda(q(0)+\delta_{L0})=0 \quad if \;\; \delta_R>0 \; e \; \delta_L=0 \quad (9c) \end{cases} \tag{9}$$

The way to proceed is to hypothesize a first value of the relative displacement of the mass, generally assumed as $q_{test}=0$, check which of the three cases reported in Eq. (9) it falls into and solve the respective equation in terms of $q(0)$; if the value of the relative displacement obtained by solving Eq. (9) coincides with the value of the hypothesized relative displacement the procedure is concluded, while if these displacements do not coincide the procedure is repeated taking as $q_{test}$ the relative displacement of the mass obtained by solving Eq. (9).

From case a) shown in Fig. 3, which is related to values $\delta_0<0$ and $e_0=0$ which lead to having values of $\delta_{0R}$ and $\delta_{0L}$ that are equal and both negative in configuration 0, it is possible to notice how the transition from configuration 0 to configuration 1 it does not involve movements of the mass; this is due to the fact that the bumpers are pre-compressed in the same way leading to the creation of two forces equal in magnitude but in opposite directions which act on the mass.

The case b) shown in Fig. 3 is instead relative to the values of $\delta_0<0$ and $e_0>0$ which lead to having values of $\delta_{0R}$ and $\delta_{0L}$ which are both negative in the 0 configuration but with $\delta_{0R}>\delta_{0L}$. This means that the left bumper has a negative gap value and is greater in absolute value than the right one and is more pre-compressed. This difference in pre-compression of the bumpers will mean that two unbalanced forces due to the bumpers act on the mass; therefore, to guarantee the balance of the mass, the damper will also have to provide its contribution through the restoring force that is generated following a relative displacement of the mass. Then, in this case the transition from configuration 0 to configuration 1 leads to a positive shift (to the right) of the mass.

The cases c) and d) shown in Fig. 3 are also related to values of $\delta_0<0$ and $e_0>0$, but in these cases this pair of values leads to having values of $\delta_{0R}$ and $\delta_{0L}$ which in configuration 0 are, respectively, positive and negative. In both cases the transition from configuration 0 to configuration 1 leads to a positive shift (to the right) of the mass, due to considerations similar to those made for the case b). For case c) the displacement suffered by the mass due to the pre-compression of the left bumper also brings the mass into contact with the right bumper (which is also compressed); however, in case d) the movement of the mass does not bring it into contact with the right bumper (which is unloaded at the initial instant).

The transition from configuration 0 to configuration 1 is a step that is always implicitly or explicitly done; in fact, if the pair of $\delta_0$ and $e_0$ leads to a pair of $\delta_0$ and $e_0$, both positive, configuration 1 will always coincide with configuration 0, while if the pair of values of $\delta_0$ and $e_0$ leads to having configurations 0 like those shown in Fig. 3, the considerations just made apply.

The nonlinear dynamic analysis will start from the initial conditions that derive from configuration 1.

Fig. 4 shows the time histories relating to the four scenarios represented in Fig. 3; hence, once configuration 0 has been defined, the nonlinear static problem that leads to configuration 1 is solved and finally the system is subjected to a harmonic forcing.

For the four time-histories reported in Fig. 4 for the dimensionless time instant $\tau=0$ it is possible to observe configuration 1; for case a) given the symmetry of the bumpers, the relative displacement of the mass is zero, while for the other cases the relative displacement of the mass is positive (the oscillator is moved to the right at the initial instant, see Fig. 3). For Fig. 4a and b the left and right gaps are both negative; this can be seen in the time history through the fact that the bumpers recover the deformation for values that have the opposite sign to the respective peak value. While for Fig. 4c and d it can be noted that the gap of the right bumper is positive while the left one is negative.

In a manner consistent with case d) in Fig. 3, in the time history reported in Fig. 4d the right bumper is not pre-compressed in configuration 1; in fact, in Fig. 4d the gap of the right bumper does not undergo deformations at the initial instant and the mass will impact for the first time against this bumper starting from a dimensionless time value $\tau=3$.

Moving from case a) to case d), the value of the eccentricity of the bumpers $e_0$ increases and -as can be seen from Fig. 4- this leads to an increasingly eccentric response.

### 3.3. Comparison between different bumpers' configurations

To show how the behavior of the system changes as the bumper configurations vary, several comparisons are made between various bumpers' configurations and the reference configuration ($\delta_0=0.06$ ed

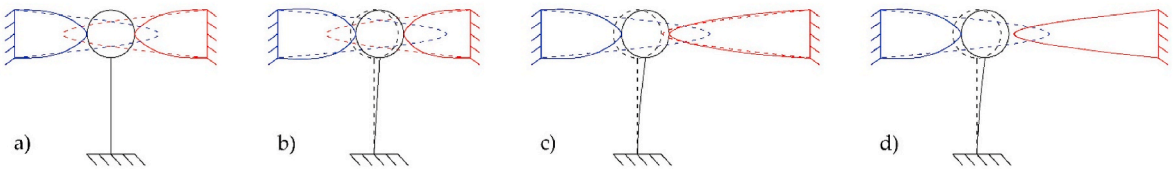


**Fig. 3.** Four of the possible scenarios that can occur due to the pseudo-random generation of $\delta_0$ and $e_0$. The dotted lines show configuration 0, i.e. the configuration that occurs following the pseudo-random generation of $\delta_0$ and $e_0$, the solid lines show configuration 1 or initial configuration of the bumpers, i.e. the equilibrium configuration that occurs following precompression of the bumpers. The case a) it is representative of a value of $\delta_0<0$ and $e_0=0$; instead the cases b), c) and d) are representative of values of $\delta_0<0$ ed $e_0>0$, in the latter three cases $\delta_0$ moving from case b) to case d) remains negative and decreases in absolute value, while $e_0$ when moving from case b) to case d) remains positive and increases in absolute value.

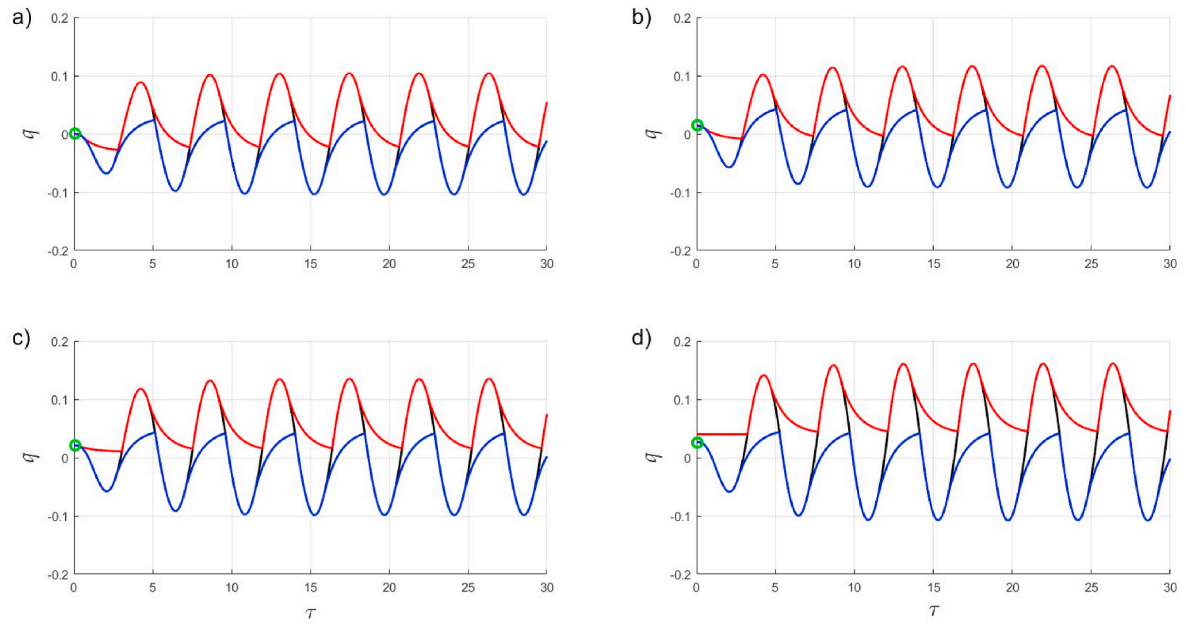


**Fig. 4.** Time histories relating to four different configurations of the bumpers, for a value of $\xi = 0.1$, $\beta = 1.42$ and for values of $\lambda = 1.14$ and $\gamma = 5.70$ that derive from the design optimal relative to the reference configuration ($\delta_0 = 0.06$, $e_0 = 0$). Time histories refer to the following pairs of $\delta_0$ and $e_0$: a) $\delta_0 = -0.06$, $e_0 = 0$, b) $\delta_0 = -0.06$, $e_0 = 0.04$, c) $\delta_0 = -0.04$, $e_0 = 0.06$, d) $\delta_0 = -0.01$, $e_0 = 0.09$; the relative displacement of the mass is shown in black, the position of the right gap in red and the position of the left bumper in blue for each instant of time The green dot indicates the initial configuration related to nonlinear static analysis.

$e_0 = 0$).

In Fig. 5a the blue and red curves refer to two configurations which have, respectively, gap excursion values $\delta_0$ larger and smaller than those of the reference configuration, while the eccentricity of the gap is identically equal to zero for in all three cases. The black curve shows the response of the reference configuration; from this figure it is possible to see how an increase in the gap excursion leads to an increase in both the relative displacement of the mass and the total force discharged to the ground, therefore leading to larger force-displacement cycles representative of a greater dissipative capacity.

In Fig. 5b the blue and red curves refer to two configurations that have negative gap excursion values $\delta_0$ and zero gap eccentricity values $e_0$, the black curve instead shows the response of the reference configuration; it is possible to note that even when the gap excursion becomes negative the same considerations made previously apply, i.e. that the area subtended by the force-displacement cycle, the maximum relative displacement of the mass and the maximum total force discharged to the ground are reduced as the gap excursion decreases.

In Fig. 5c and d it is analyzed how the eccentricity of the gap, positive and negative, is reflected in the response. This is done both for values of

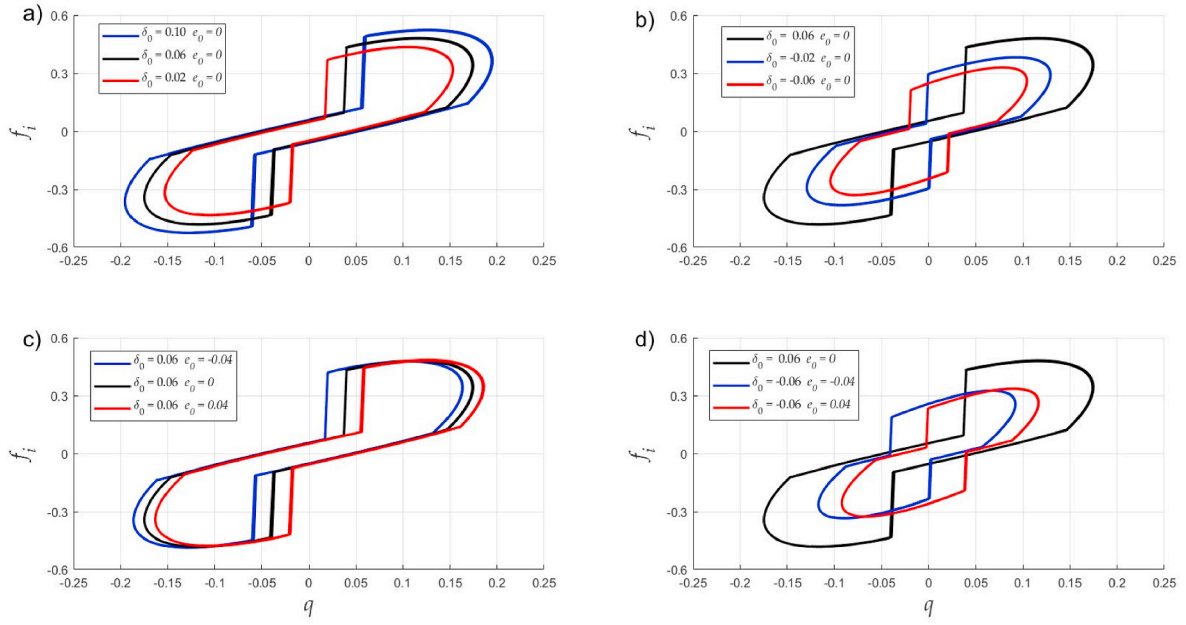


**Fig. 5.** Comparison between different force-displacement cycles with the reference configuration ($\delta_0 = 0.06$, $e_0 = 0$), for a value of $\xi = 0.1$, $\beta = 1.42$ and for values of $\lambda = 1.14$ and $\gamma = 5.70$ which derive from the optimal design relative to the reference configuration ($\delta_0 = 0.06$, $e_0 = 0$). In all the figures, the black curve is related to the reference configuration, while the blue and red curves are related to bumpers configurations that are compared with the reference one.

the gap excursion equal to that of the reference configuration (Fig. 5c) and for negative gap excursion values (Fig. 5d). From these figures it is possible to see how the eccentricity of the gap leads to a translation in the direction of the stiffness of the damper of the force-displacement cycles. In fact, for the same gap excursion the area subtended by the force-displacement cycle remains the same. This translation is due to the response quantities which also become eccentric following the eccentricity of the gap.

## 4. Effect of gap size uncertainty on the nonlinear dynamic response

The main objective of this section is to show how the uncertainties that exist on the parameters $\delta_0$ and $e_0$ are reflected on the response; in fact, we are going to probe how sensitive the system is to variations in these parameters.

To give a better understanding of the results that will be shown, the dimensionless parameters $\delta_0$ and $e_0$ are written as a function of the dimensional parameters, in order to understand which physical parameters we are planning of varying:

$$\begin{cases} \delta_0 = \dfrac{(G_{0d} + G_{0s})\omega^2}{A_g R_{d,max}} & (10a) \\ e_0 = \dfrac{(G_{0d} - G_{0s})\omega^2}{A_g R_{d,max}} & (10b) \end{cases} \tag{10}$$

Assuming that both the parameters $\omega^2$ and $R_{d,max}$ of the SDOF system and the action parameter $A_g$ are known, the uncertainties that affect the dimensionless parameters $\delta_0$ and $e_0$ are exclusively linked to uncertainties that affect the physical parameters $G_{0R}$ and $G_{0L}$ (shown in Fig. 1).

The uncertainties linked to the value of the two gaps $G_{0R}$ and $G_{0L}$ mainly derive from errors in the positioning of the bumpers or from accidental position variations that can occur subsequently.

### 4.1. Generation of the input parameters $\delta_0$ and $e_0$.

The robustness analysis conducted is not a simple parametric analysis in which a range of variation is set for the parameters $\delta_0$ and $e_0$ and all possible cases are analyzed, but in the following analysis the pairs of values $\delta_0$ and $e_0$ are generated in a pseudo-random way according to probabilistic criteria.

The way in which the analysis is conducted consists in fixing the pair of values $\delta_0$ and $e_0$, which we will later call the reference configuration (it would be the desired configuration of the bumpers). From this configuration the dimensionless stiffness $\lambda$ and the dimensionless damping $\gamma$ are obtained through the optimal design procedure, which consists in entering the optimality curve with a value of $\delta = \delta_0/2$ thus obtaining the parameter $\lambda_R = \lambda_L = \lambda$. Known $\lambda$, the parameter $\gamma_R = \gamma_L = \gamma$ is obtained through the optimality relation. Finally, different pairs of values $\delta_0$ and $e_0$, also called "configurations", are generated in a pseudo-random way. Therefore, for all the configurations generated in a pseudo-random way, the values of $\lambda$ and $\gamma$ are those that derive from the optimal design carried out with the reference configuration.

In this article the pairs of values $\delta_0$ and $e_0$ are generated in a pseudo-random way (MATLAB function *random*): both a vector of values for $\delta_0$ and a vector of values for $e_0$ are generated, both of which are arranged according to a normal probability distribution; therefore the $j$-th component of the vector $\delta_0$ is associated with the $j$-th component of the vector $e_0$, generating the $j$-th configuration.

To make a comparison between a histogram and a probability density function (pdf), it is necessary to scale the histogram in a way consistent with the probability density function, therefore since the area under the pdf is equal to one, also the area under the histogram must be equal to one.

Fig. 6 shows how the values of $\delta_0$ and $e_0$ generated in a pseudo-random way, represented by the blue histogram, are arranged according to a normal probability distribution, which has the same mean and standard deviation as the values of $\delta_0$ and $e_0$ generated. The values of $\delta_0$ and $e_0$ generated have an average value that tends to the value of the reference configuration, while the standard deviation is assumed to be the same for both parameters.

In this paper, the value of the standard deviation is chosen in such a way that almost all of the values of $\delta_0$ and $e_0$ generated fall in a range between $\mp 0.1$ the value of the reference configuration, thus allowing the behavior of the system to be analyzed even for values of the gap parameters that are significantly different than that of the reference configuration.

### 4.2. Confidence zone

For each of the generated bumper configurations, the Pseudo-Resonance Curves (PRCs) are worked out for the eight response quantities reported in Eqs. (5)–(8).

The PRCs are traced by subjecting the system shown in Fig. 1 to a sine-type action with dimensionless frequency $\beta$ varying over time and with constant dimensionless acceleration $a_G$. Therefore, we start from the minimum value of $\beta$ considered, bring the system to steady state conditions and through the relations reported in Eqs. (5)–(8) the first point of the curve is plotted, after that the value of the dimensionless frequency $\beta$ is changed, increasing it by an appropriate increment $\Delta\beta$, and the system is brought again to steady state conditions starting from the initial conditions that derive from the time history obtained with the previous $\beta$. This is done until reaching a maximum value of $\beta$, once this value of $\beta$ is reached we will return to the minimum $\beta$ value by reducing the frequency of the forcing of a decrement $\Delta\beta$ at each step. The PRCs

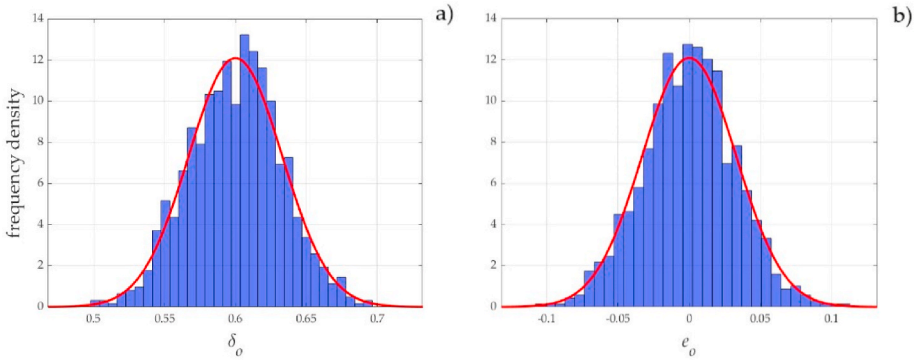


**Fig. 6.** Comparison of the histogram of the input parameters ($\delta_0$ and $e_0$) generated pseudo-randomly with the normal type probability density function for the reference configuration $\delta_0 = 0.6$ and $e_0 = 0$; in graph a) the histogram of the frequency densities of the gap excursion $\delta_0$ and the comparison with the relative probability density function (red curve) are shown; similarly in graph b) the same comparison is shown but made with the eccentricity of the gap $e_0$.

traced in this way, in addition to providing information about the system in steady state conditions, also allow us to understand how much the system depends on the initial conditions.

The presence of an uncertainty in the input parameters $\delta_0$ and $e_0$ is reflected in an uncertainty in the output parameters, i.e. in the response quantities; this leads to responses that are not deterministic but which can take on values within a certain range, called confidence zone.

The graphs shown in Fig. 7 are related to a specific reference configuration ($\delta_0 = 0.6$ and $e_0 = 0$) but it can be assumed as representative of an entire range of reference configurations, i.e. for all those reference configurations that present $\delta_0 > 0.38$ and $e_0 = 0$.

Fig. 7 shows the Pseudo-Resonance Curves for both the reference configuration (red curve) and for the gap configurations generated in a pseudo-random way (PRCs of 1000 configurations represented by black curves). The blue points represented in the various figures identify the range of $\beta$ values for which the collision occurs for the reference configuration. As can be seen from these figures for some values of $\beta$ the response is not unique but takes on different values going to define the confidence zone, which takes on a length defined by the range $0.30 \leq \beta \leq 1.35$ and an width that in general does not remain constant, showing how there are some values of $\beta$ that are more sensitive than others to uncertainties.

The graph shown in Fig. 7$a_1$ shows the PRCs of excursion of the relative displacement of the mass. The width of the confidence zone does not remain constant with $\beta$ and shows the maximum width for the $\beta$ of resonance ($\beta = 1.09$) where it is equal to 0.081; finally, it is possible to note how for a value of $\beta$ equal to 1.2 this width tends to zero.

The graph shown in Fig. 7$a_2$ shows the PRCs of the eccentricity of the relative displacement of the mass. The width of the confidence zone does not remain constant with $\beta$ and shows maxima in correspondence with two values of $\beta$, i.e. for $\beta = 0.5$ and $\beta = 1.15$ where it turns out to be, respectively, equal to 0.022 and 0.028; finally it is possible to notice how this graph shows a certain symmetry with respect to the axis $\eta_{d,ecc} = 0$.

The graph shown in Fig. 7$b_1$ shows the PRCs of the excursion of the absolute acceleration of the mass. The width of the confidence zone does not remain constant with $\beta$ and shows the maximum width for the $\beta$ of resonance ($\beta = 1.08$) where it is equal to 0.082; finally, it is possible to note how, also in this case, for a value of $\beta$ approximately equal to 1.18 the width of the confidence zone tends to zero.

The graph shown in Fig. 7$b_2$ shows the PRCs of the eccentricity of the absolute acceleration of the mass. The width of the confidence zone does not remain constant with $\beta$ and shows maximums near the two blue points, i.e. for $\beta = 0.7$ and $\beta = 1.25$ where it is, respectively, equal to 0.064 and 0.093; finally it is possible to notice how this graph shows a certain symmetry with respect to the axis $\eta_{a,ecc} = 0$.

The graph shown in Fig. 7$c_1$ shows the PRCs of the excursion of the deformations of the bumpers. The width of the confidence zone does not remain constant with $\beta$ and shows the maximum width for a value of $\beta = 1.25$ where it is equal to 0.102.

The graph shown in Fig. 7$c_2$ shows the PRCs of the eccentricity of the deformations of the bumpers. The width of the confidence zone remains approximately constant for most of its width where it is equal to 0.010, also in this case it is possible observe a certain symmetry with respect to the axis $\eta_{B,ecc} = 0$.

The graph shown in Fig. 7$d_1$ shows the PRCs of the excursion of the contact forces of the bumpers. The width of the confidence zone does not

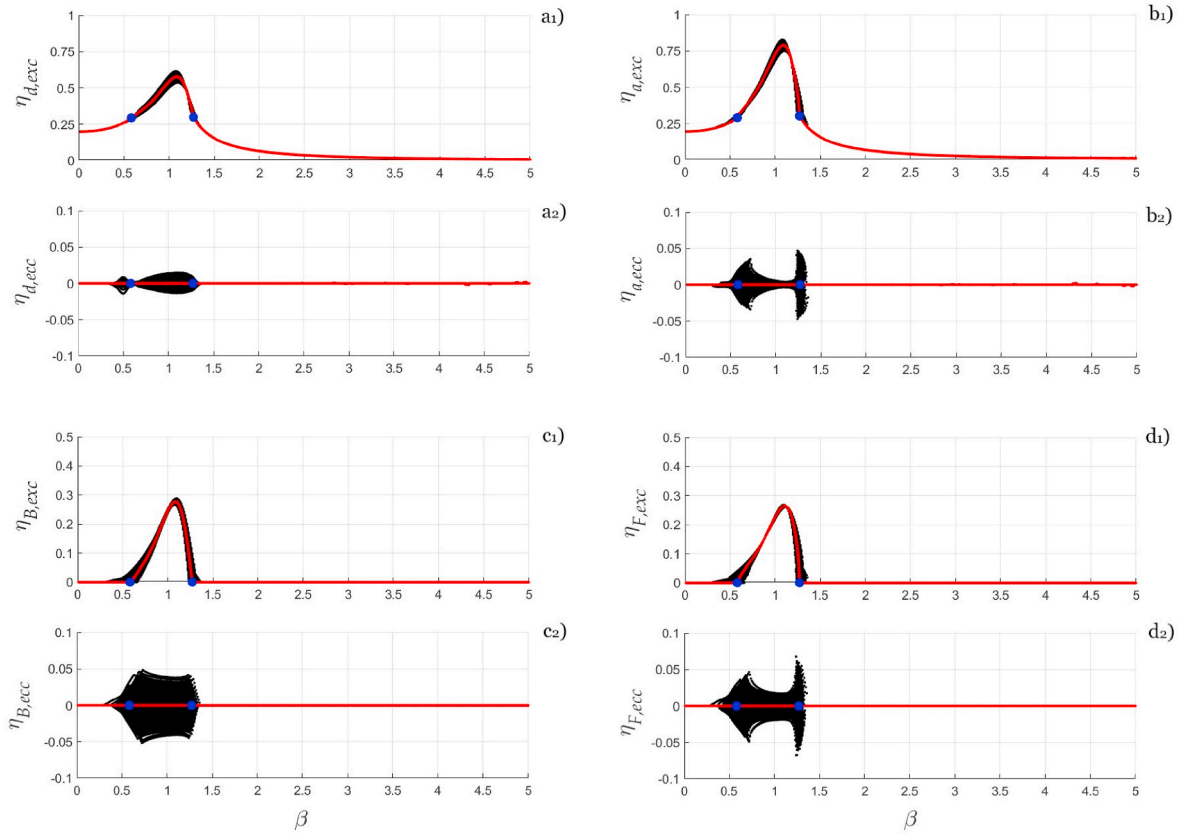


**Fig. 7.** Pseudo-Resonance Curves obtained for a value of $\xi = 0.1$, for values of $\lambda = 0.45$ and $\gamma = 2.26$ which derive from the optimal design relative to the reference configuration ($\delta_0 = 0.6$ and $e_0 = 0$). In a1) and a2) the PRCs of the excursion and eccentricity of the relative displacement of the mass are reported; in b1) and b2) the PRCs of the excursion and eccentricity of the absolute acceleration of the mass are reported; in c1) and c2) the PRCs of the excursion and eccentricity of the deformations of the bumpers are reported; in d1) and d2) the PRCs of the excursion and eccentricity of the contact forces of the bumpers are reported. In all graphs, the red curves represent the PRCs of the reference configuration, the blue points delimit the range of β values for which the collision occurs in the reference configuration; finally, the black curves represent the response of the pseudo-random configurations.

remain constant with $\beta$ and shows the maximum width for a value of $\beta = 1.25$ where it assumes a value equal to 0.146; finally, it is possible to note that in this case there are two values for which the confidence zone tends to zero, i.e. for $\beta$ equal to 0.89 and 1.14.

The graph shown in Fig. 7$d_2$ shows the PRCs of the eccentricity of the contact forces of the bumpers. The width of the confidence zone does not remain constant with $\beta$ but shows maxima near the two blue points, i.e. for $\beta = 0.72$ end $\beta = 1.24$ where it turns out to be, respectively, equal to 0.096 and 0.135; also in this case the graph shows a certain symmetry with respect to the axis $\eta_{F,ecc} = 0$.

The graphs shown in Fig. 8 are related to a given reference configuration ($\delta_0 = 0.06$ ed $e_0 = 0$) but it can be assumed as representative of an entire range of reference configurations $\delta_0 \leq 0.38$ and $e_0 = 0$. Many of the pseudo-random configurations analyzed in Fig. 8 have negative gaps, so these results also show how the system responds to such configurations.

Fig. 8 shows the Pseudo-Resonance Curves for both the reference configuration (red curve) and for the gap configurations generated in a pseudo-random way (PRCs of 1000 configurations represented by black curves). The blue points represented in the various figures identify the range of $\beta$ values for which the collision occurs for the reference configuration. As can be seen from these figures, for the entire range of $\beta$ values the response is not unique but takes on different values, defining the confidence zone, which takes on a length equal to the entire range of $\beta$ and a width which in general does not remain constant, showing how there are some values of $\beta$ that are more sensitive to uncertainties than others.

The graph shown in Fig. 8$a_1$ shows the PRCs of the excursion of the relative displacement of the mass. The width of the confidence zone does not remain constant with $\beta$ but shows the maximum width near the value of $\beta$ for which resonance occurs ($\beta = 1.30$) and is equal to 0.134, the point at which the confidence zone tends to zero is not so clear but can be identified near a value of $\beta$ equal to 2.1.

The graph shown in Fig. 8$a_2$ shows the PRCs of the eccentricity of the relative displacement of the mass. The width of the confidence zone can be assumed constant with a good approximation for the entire range of $\beta$ with a width equal to 0.056. Finally, it is possible to notice how this graph shows a certain symmetry with respect to the axis $\eta_{d,ecc} = 0$.

The graph shown in Fig. 8$b_1$ shows the PRCs of the excursion of the absolute acceleration of the mass. The width of the confidence zone does not remain constant with $\beta$ and shows its maximum widths in correspondence with two points, the first near the value of $\beta$ for which the resonance occurs ($\beta = 1.34$) where it presents a value of 0.264, while the second turns out to be $\beta = 2$ with an width equal to 0.219; also in this case the point at which the confidence zone tends to zero is not so clear but can be identified near a value of $\beta$ equal to 1.7.

The graph shown in Fig. 8$b_2$ shows the PRCs of the eccentricity of the absolute acceleration of the mass. The width of the confidence zone does not remain constant with $\beta$ but shows a first maximum point for $\beta = 0.6$ where it takes on a value of 0.057, after which it gradually reduces until reaching a width of 0.019 which remains constant until value of $\beta = 1.9$ where it shows a sharp increase assuming a value equal to 0.128, finally it is possible to notice how this graph shows a certain symmetry with respect to the axis $\eta_{a,ecc} = 0$.

The graph shown in Fig. 8$c_1$ shows the PRCs of the excursion of the

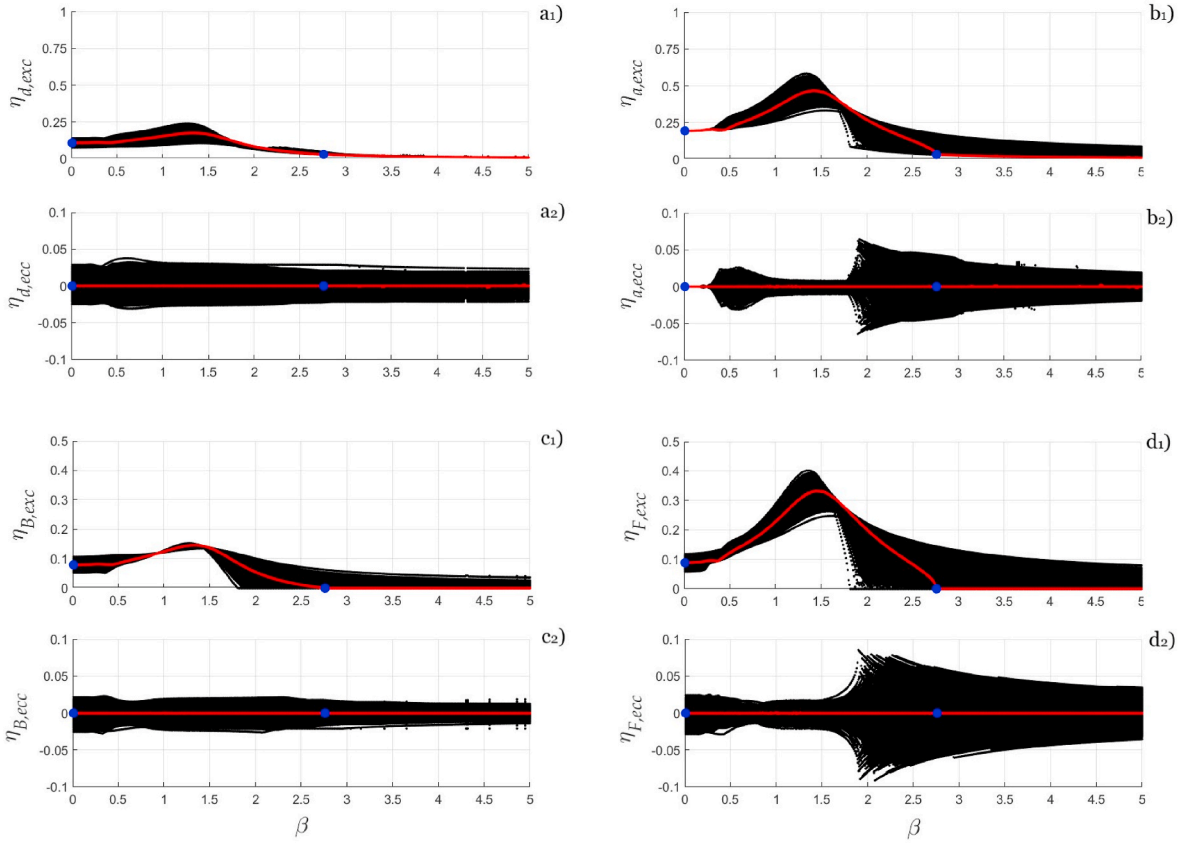


**Fig. 8.** Pseudo-Resonance Curves obtained for a value of $\xi = 0.1$, for values of $\lambda = 1.14$ and $\gamma = 5.70$ which derive from the optimal design relative to the reference configuration ($\delta_0 = 0.06$ and $e_0 = 0$). In $a_1$) and $a_2$) the PRCs of the excursion and eccentricity of the relative displacement of the mass are reported, in $b_1$) and $b_2$) the PRCs of the excursion and eccentricity of the absolute acceleration of the mass are reported, in c1) and $c_2$) the PRCs of the excursion and eccentricity of the deformations of the bumpers are reported, in $d_1$) and $d_2$) the PRCs of the excursion and eccentricity of the contact forces of the bumpers are reported. In all graphs, the red curves represent the PRCs of the reference configuration, the blue points delimit the range of β values for which the collision occurs in the reference configuration; finally, the black curves represent the response of the pseudo-random configurations.

deformations of the bumpers. The width of the confidence zone does not remain constant with $\beta$ and shows the maximum width for a value of $\beta = 1.8$ where it is equal to 0.117; in this case the points in which the width of the confidence zone tends to zero are two and they are localized for $\beta$ values of 0.95 and 1.45.

The graph shown in Fig. 8$c_2$ shows the PRCs of the eccentricity of the deformations of the bumpers. The width of the confidence zone can be assumed with a good approximation to be constant for the entire range of $\beta$ with a width equal to 0.043; also, in this case it is possible to observe a certain symmetry with respect to the axis $\eta_{B,ecc} = 0$.

The graph shown in Fig. 8$d_1$ shows the PRCs of the excursion of the contact forces of the bumpers. The width of the confidence zone does not remain constant with $\beta$ and shows its maximum widths in correspondence with two points, the first near the value of $\beta$ for which the resonance occurs ($\beta = 1.35$) where it presents a value of 0.172, while the second is $\beta = 1.8$ with an width equal to 0.257, also in this case the point at which the confidence zone tends to zero is not so clear but can be identified near a value of $\beta$ equal to 1.7.

The graph shown in Fig. 8$d_2$ shows the PRCs of the eccentricity of the contact forces of the bumpers. The width of the confidence zone remains approximately constant up to a value of $\beta = 1.9$ where it shows a sharp increase assuming a value equal to 0.175, also in this case the graph shows a certain symmetry with respect to the axis $\eta_{F,ecc} = 0$.

Comparing the PRCs relating to the two reference configurations (red curves in the figure) of Figs. 7 and 8, it is possible to see how a reduction in the excursion of the gap $\delta_0$ leads to lower excursions of the relative displacements and absolute accelerations of the mass. The excursions of the deformations of the bumpers are also smaller as they decrease, while the excursion of the contact forces of the bumpers are larger for the reference configuration shown in Fig. 8. In all cases the eccentricity of the various response quantities is always zero; this result is a direct consequence of the optimal design carried out. For Fig. 8 it is possible to notice how the first blue point is positioned for a value of $\beta = 0$, this condition, which occurs for the first time for a value of $\delta_0 = 0.38$, has been identified as a watershed between two different types of results: those similar to the results in Fig. 7 and those similar to the results in Fig. 8.

Moving on to analyze the various confidence zones, it is possible to notice how for all the graphs shown in Fig. 7 the confidence zones always disappear near the two blue points, while for all the graphs shown in Fig. 8 the confidence zones are present throughout the range of $\beta$. Furthermore, for the graphs shown in Fig. 8 the confidence zones, in addition to being markedly longer, are also wider than those shown in the graphs shown in Fig. 7. From these considerations it is possible to deduce that systems that have a reference configuration characterized by smaller gap excursion values are more sensitive to uncertainties than those systems that have a reference configuration that present a greater gap excursion.

### 4.3. Symmetry of the eccentricity of the response quantities

From Figs. 7 and 8 it is possible to see how the graphs of the eccentricities of all the response quantities show a fairly symmetrical trend. Therefore, we want to verify whether this symmetry derives exclusively from bumper configurations that have the same gap excursion value but eccentricity of the opposite sign.

The Pseudo-Resonance Curves shown in Figs. 7 and 8 were obtained by carrying out a sweep of the $\beta$ value both forwards and backwards, taking the steady-state values of the previous $\beta$ as initial conditions of the subsequent $\beta$; this way of proceeding, although it allows us to probe how much the system has a more or less strong dependence on the initial conditions, can lead to different results based on the initial conditions. The first thing to do to better highlight this possible symmetry of the eccentricity of the response is to trace the PRCs always taking the same initial conditions for each value of $\beta$.

Furthermore, the pseudo-random generation of the values of $\delta_0$ and $e_0$ inevitably leads to not having configurations with the same gap excursion values but with eccentricities of the opposite sign, as can be seen from Fig. 6 in which the graphs of $\delta_0$ and $e_0$ are not perfectly symmetrical. The second thing to do is therefore to ensure that each value of $\delta_0$, generated in a pseudo-random way, is associated with a value of $e_0$, also generated in a pseudo-random way, equal in magnitude but of opposite sign.

By ensuring these two conditions it is possible to verify whether there is perfect symmetry in the response eccentricity graphs.

Fig. 9 shows the PRCs of the eccentricity of the various response quantities both for case a), which is relative to a reference configuration of $\delta_0 = 0.6$ and $e_0 = 0$, and for case b), which is relative to a reference configuration of $\delta_0 = 0.06$ and $e_0 = 0$. For both cases all response quantities show perfect symmetry.

The graphs shown in Fig. 9$a_1$ and Fig. 9$b_1$ relate to the eccentricity of the relative displacement of the mass. From Fig. 9$b_1$ it is possible to see how configurations that have values of $e_0 > 0$ (and similarly $e_0 < 0$) are associated with eccentricities of the response quantity which are also positive (negative). Instead from Fig. 9$a_1$ it is possible to notice how there are ranges of $\beta$ in which the configurations that have values of $e_0 > 0$ (and similarly $e_0 < 0$) present an eccentricity of the response quantity which is also positive (negative), while for other ranges of $\beta$ a real change in behavior occurs, i.e. the configurations that have values of $e_0 > 0$ (and similarly $e_0 < 0$) present an eccentricity negative (positive) of the response quantity.

Behaviors similar to those just described are also present for Fig. 9$a_2$ and Fig. 9$b_2$, which relate to the eccentricity of the absolute acceleration of the mass.

In the graphs reported in Fig. 9$a_3$ and Fig. 9$b_3$ which are related to the eccentricity of the deformations of the bumpers, and in those reported in Fig. 9$a_4$ and Fig. 9$b_4$ which are related to the eccentricity of the contact forces of the bumpers, it is possible to observe how the configurations that have values of $e_0 > 0$ (represented by the PRCs in green) present a negative eccentricity of the response quantity. Vice versa the configurations that have values of $e_0 < 0$ (represented by the PRCs in red) present a positive eccentricity of the response quantity.

Fig. 10 shows the PRCs of the excursion of the absolute acceleration of the mass for case b), i.e. the one relating to a reference configuration $\delta_0 = 0.06$ and $e_0 = 0$. In drawing the graph, all the responses relating to pseudo-random configurations that have values of $e_0 > 0$ were first plotted in green, and then all the responses relating to values of $e_0 < 0$ are plotted in red. As one can see from this graph there is a perfect overlap of the green PRCs and the red ones, as all the green PRCs are covered by the red PRCs. Results similar to those shown in Fig. 10 are obtained for all response excursions for both cases a) and b). From these results it can be deduced that the response excursions are not affected by the sign of the gap eccentricity, as the results obtained for positive eccentricity values of the gap are obtained exactly for negative eccentricity values of the gap.

### 4.4. Behaviour change points

In Fig. 9 the PRCs of the eccentricities of the various responses have been reported. This figure, in addition to containing information of the output (i.e. of the various response quantities), also contains information of an input quantity (the eccentricity of the gap $e_0$). This was done by representing the PRCs with an $e_0 > 0$ in green and the PRCs with an $e_0 < 0$ in red. Similarly, the figures shown in this section, in addition to containing output information (mainly the excursion of the various response quantities), also contain information of an input quantity, which in this case is the gap excursion.

Fig. 11 shows the PRCs of the excursion of the various response quantities both for case a), which is relative to a reference configuration of $\delta_0 = 0.6$ and $e_0 = 0$, and for case b), which is relative to a reference configuration of $\delta_0 = 0.06$ and $e_0 = 0$. The orange PRCs refer to bumper

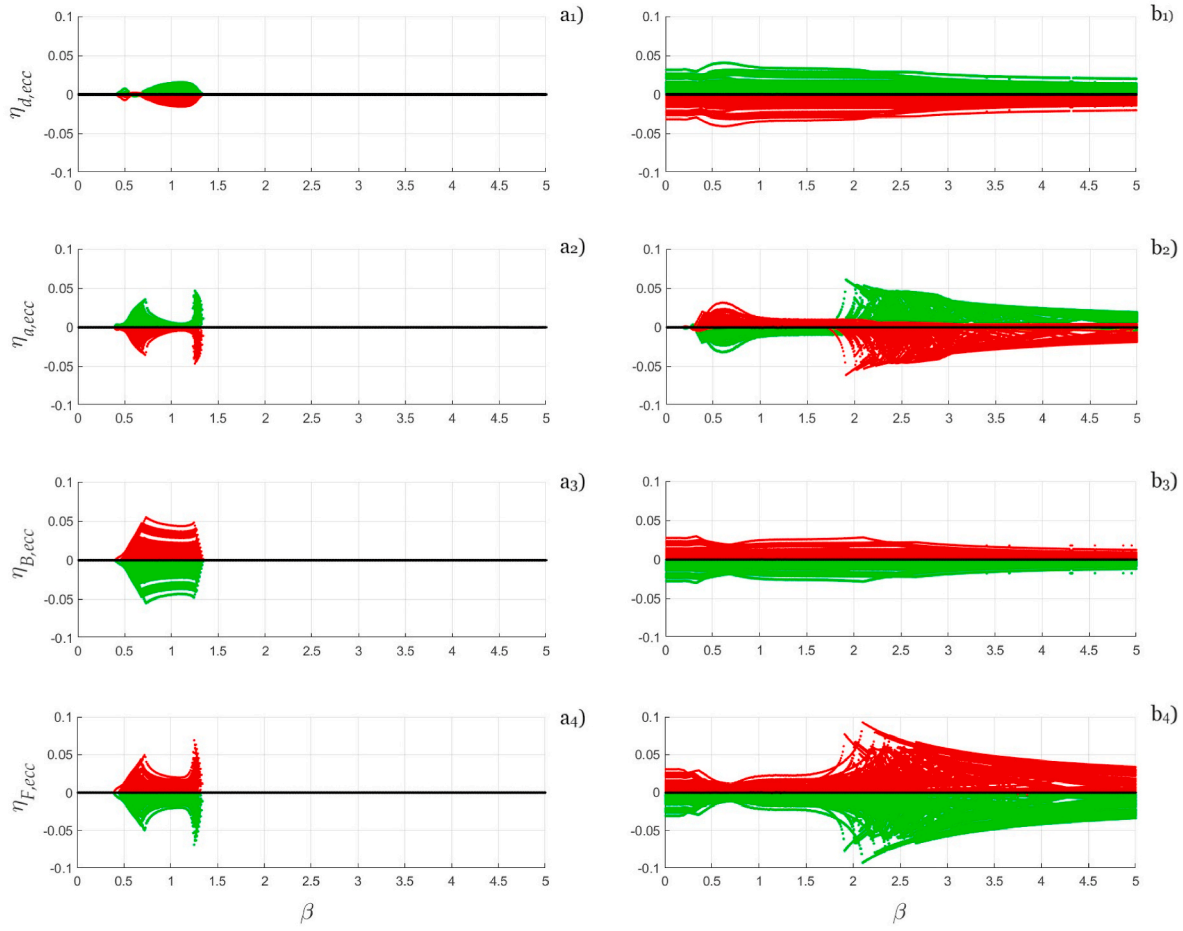


**Fig. 9.** Pseudo-Resonance Curves obtained for a value of $\xi = 0.1$, obtained for two reference configurations (for case a): $\delta_0 = 0.6$ and $e_0 = 0$, for case b): $\delta_0 = 0.06$ ed $e_0 = 0$) and for values of $\lambda$ and $\gamma$ that derive from the optimal design relating to the respective reference configurations (for case a): $\lambda = 0.45$ and $\gamma = 2.26$; for case b): $\lambda = 1.14$ and $\gamma = 5.70$. In a1), a2), a3) and a4) (and similarly in b1), b2), b3) and b4)) the PRCs of the eccentricity of the relative displacement and of the absolute acceleration of the mass, of the deformation and of the contact forces of the bumpers are reported. In all graphs, the curves in black represent the PRCs relating to the reference configuration, the PRCs relating to configurations with positive gap eccentricity are shown in green, while in red those relating to a negative gap eccentricity.

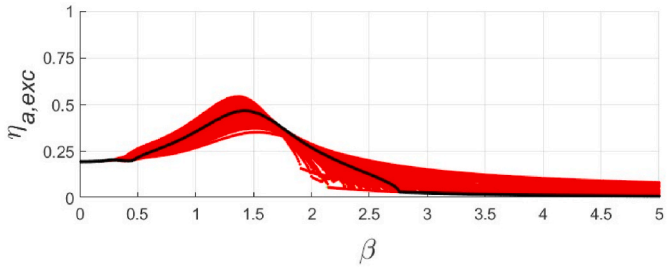


**Fig. 10.** Pseudo-Resonance Curves of the excursion of the absolute acceleration of the mass obtained for a value of $\xi = 0.1$ for values of $\lambda = 1.14$ and $\gamma = 5.70$ that derive from the optimal design relative to the reference configurations ($\delta_0 = 0.06$ and $e_0 = 0$). The curves in black represent the PRCs relating to the reference configuration, in green the PRCs relating to configurations with positive gap eccentricity are shown, while in red those relating to a negative gap eccentricity.

configurations that present a gap excursion value $\delta_0$ greater than that of the reference configuration, while the light blue curves refer to those configurations that present a $\delta_0$ lower than that of the reference configuration.

Commenting on Figs. 7 and 8, we noticed the presence, for some response quantities, of some values of $\boldsymbol{\beta}$ near which the confidence zone showed a more or less marked narrowing; from Fig. 11 it is possible to see how near these restrictions there is a change in the behavior of the confidence zones.

The graphs shown in Fig. 11$a_1$ and Fig. 11$b_1$ are related to the excursion of the relative displacement of the mass. From Fig. 11$a_1$ it is possible to notice how in correspondence with a value of $\beta = 1.2$ there is a point of change in behavior characterized by the fact that the width of the confidence zone tends to zero; for values of $\beta < 1.2$ the configurations with values of $\delta_0$ greater than that of the reference configuration (and similarly, the configurations with values of $\delta_0$ lower than that of the reference configuration) show a greater (smaller) response than that of the reference configuration, while for values of $\beta > 1.2$ the configurations with values of $\delta_0$ greater than that of the reference configuration (and similarly, configurations with values of $\delta_0$ smaller than that of the reference configuration) show a smaller (greater) response than that of the reference configuration. Instead, from Fig. 11$b_1$ it is possible to see how up to a value of $\beta = 1.7$ the configurations with $\delta_0$ greater than that of the reference configuration present responses greater than the reference one. For values of $1.7 < \beta < 2.1$ these configurations present lower responses with respect to the reference one, while for values of $\beta > 2.1$ they return to having greater responses than the reference one. Configurations with values of $\delta_0$ lower than that of the reference configuration present responses lower than the reference one up to a value of $\beta = 2.1$, however after this point of change in behavior they present responses greater than the reference one.

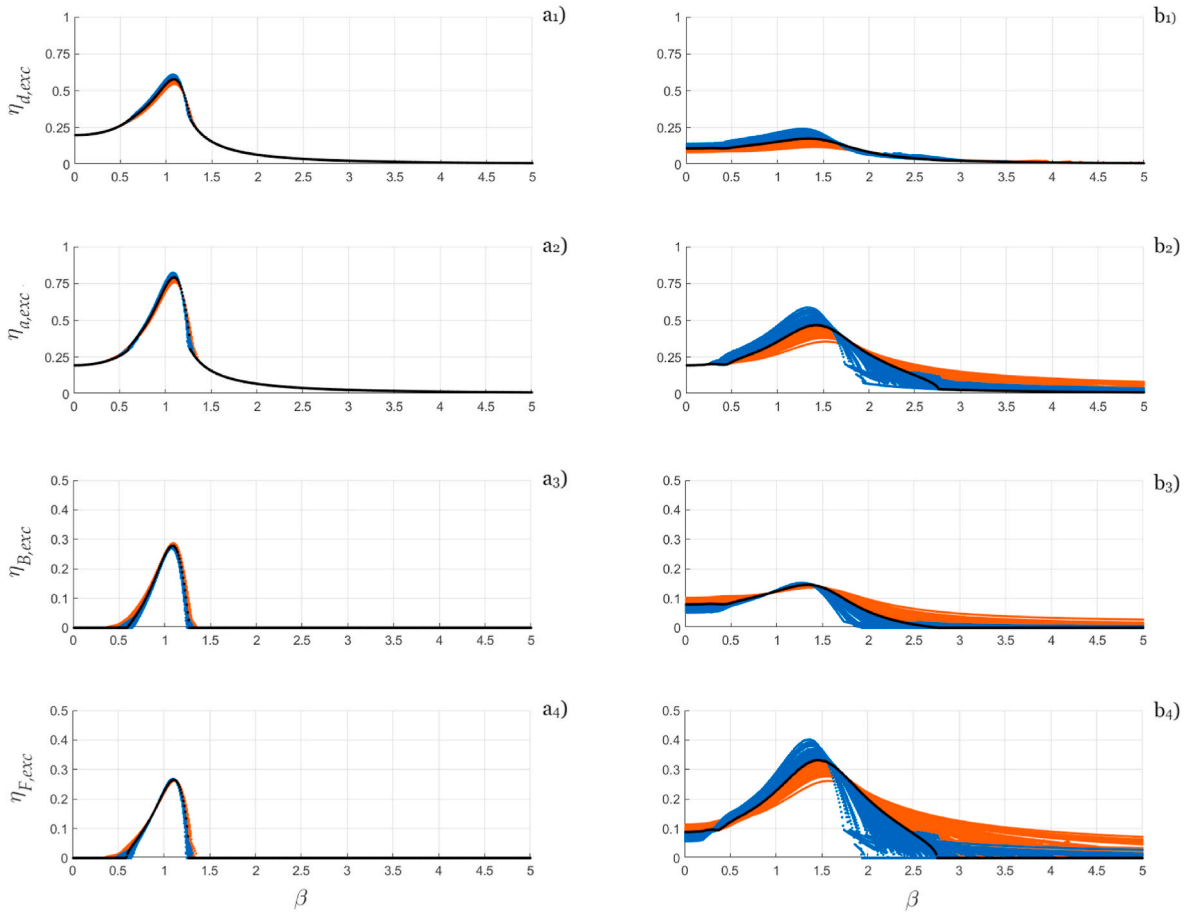


**Fig. 11.** Pseudo-Resonance Curves obtained for a value of $\xi = 0.1$, obtained for two reference configurations for case a): $\delta_0 = 0.6$ and $e_0 = 0$, for case b): $\delta_0 = 0.06$ and $e_0 = 0$, and for values of $\lambda$ and $\gamma$ that derive from the optimal design relating to the respective reference configurations for case a): $\lambda = 0.45$ and $\gamma = 2.26$, for the case b): $\lambda = 1.14$ and $\gamma = 5.70$). In a1), a2), a3) and a4) (and similarly in b1), b2), b3), b4)) the PRCs of the excursion of the relative displacement and of the absolute acceleration of the mass, of the deformation and the contact forces of the bumpers are reported. In all the graphs, the curves in black represent the PRCs relating to the reference configuration, in orange the PRCs relating to configurations which present a gap excursion larger than those of the reference configuration are shown, while in blue those relating to a gap excursion smaller than that of the reference configuration.

The graphs shown in Fig. 11$a_2$ and Fig. 11$b_2$ are related to the excursion of the absolute acceleration of the mass. These graphs show similar behavior to that of the graphs shown in Fig. 11$a_1$ and Fig. 11$b_1$; the only differences derive from the different position of the behavior change points, which for the graph shown in Fig. 11$a_2$ occurs for a value of $\beta = 1.18$. For the graph shown in Fig. 11$b_2$, the configurations with $\delta_0$ greater than that of the reference configuration present two points of change in behavior which occur for $\beta = 1.7$ and $\beta = 2.5$, while the configurations with $\delta_0$ less than that of the reference one present only one point of change in behavior for $\beta = 1.7$.

The graphs shown in Fig. 11$a_3$ and Fig. 11$b_3$ relate to the range of deformations of the bumpers. The graph shown in Fig. 11$a_3$ presents a single point of change in behavior at $\beta = 0.65$; instead, the graph shown in Fig. 11$b_3$ presents two points of change in behavior, characterized by the fact that the width of the confidence zone tends to zero, corresponding to $\beta = 0.9$ and $\beta = 1.4$.

Finally, the graphs shown in Fig. 11$a_4$ and Fig. 11$b_4$ relate to the excursion of the contact forces of the bumpers. The graph shown in Fig. 11$a_4$ presents a first point of change in behavior at $\beta = 0.65$ and two other points, characterized by the fact that the width of the confidence zone tends to zero, for $\beta = 0.9$ and $\beta = 1.1$; instead the graph shown in Fig. 11$b_4$ presents three points of change in behavior corresponding to $\beta = 0.35$, $\beta = 1.75$ and $\beta = 2.6$.

Fig. 12 shows the PRCs of the eccentricity of the absolute acceleration of the mass for case a), the one relating to a reference configuration

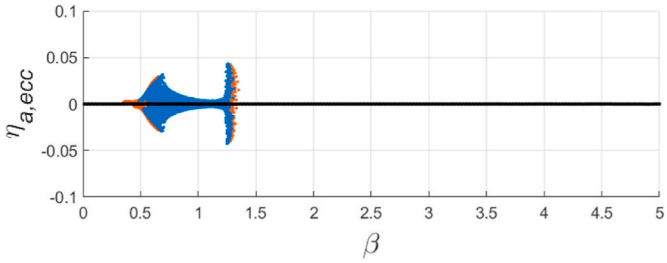


**Fig. 12.** Pseudo-Resonance Curves of the eccentricity of the absolute acceleration of the mass obtained for a value of $\xi = 0.1$, for values of $\lambda = 0.45$ and $\gamma = 2.26$ that are derived from the optimal design relative to the reference configurations ($\delta_0 = 0.6$ ed $e_0 = 0$). The curves in black represent PRCs relative to the reference configuration, in orange are PRCs relative to configurations that have a larger gap excursion than those of the reference configuration, and in light blue those relative to a smaller gap excursion than that of the reference configuration.

$\delta_0 = 0.6$ and $e_0 = 0$; from this graph it is possible to see how the PRCs obtained for values of $\delta_0$ 0 greater than that of the reference configuration (orange curves) provide very similar results to those of the PRCs which have $\delta_0$ values lower than that of the reference configuration (blue curves). Results similar to those shown in Fig. 12 are obtained for all response eccentricities for both cases a) and b). From these results it

can be deduced that the response excursions are not excessively affected by variations in gap excursion.

### 4.5. Relationship between input and output quantities

The considerations made up to now have highlighted how the link between the input quantities ($\delta_0$ and $e_0$) and the output quantities (the various response quantities) does not remain constant either when $\beta$ varies or the value of $\beta$, however, from these graphs it is still quite complicated to understand the link between the input and output quantities.

In this section, the link between the input and output quantities is shown through level curve graphs.

Fig. 13 shows the relationship between the parameters $\delta_0$ and $e_0$ and the response quantities excursion and eccentricity of the contact force of the bumpers, for the case which has as reference configuration $\delta_0 = 0.6$ and $e_0 = 0$ and for a value of $\beta = 1.05$. For this value of $\beta$ the collision occurs in all the configurations of the bumpers generated in a pseudo-random way.

The contour plots depicted in the graph shown in Fig. 13a show a pseudo-vertical trend and perfect symmetry with respect to the axis $e_0 = 0$. The pseudo-vertical trend of the contour plots shows how, once a value of $\delta_0$, is fixed, even a fairly significant variation in $e_0$ does not lead to large variations in the response; the perfect symmetry of the response with respect to the $e_0 = 0$, axis, which had already been glimpsed in Fig. 10, shows how, having fixed a value of $\delta_0$ and the value of $e_0$ in modulus, the positive and negative eccentricity of the gap provide exactly the same answer.

The contour plots shown in the graph shown in Fig. 13b show a pseudo-horizontal trend and perfect symmetry with respect to the $e_0 = 0$ axis. The pseudo-horizontal trend of the contour plots shows how, once a value of $e_0$, is fixed, even a fairly significant variation in $\delta_0$ does not lead to large variations in the response; the perfect symmetry of the curves with respect to the axis $e_0 = 0$, which had already been glimpsed in Fig. 9, shows how, having fixed a value of $\delta_0$ and the value of $e_0$ in modulus, the positive and negative eccentricity of the gap provide exactly the same answer, equal in form but of opposite sign.

Fig. 14 shows the relationship between the parameters $\delta_0$ and $e_0$ and the response quantities excursion and eccentricity of the contact force of the bumpers, for the case which has as reference configuration $\delta_0 = 0.6$ and $e_0 = 0$ and for a value of $\beta = 1.20$. Also in this case, for this value of $\beta$ the collision occurs in all the configurations of the bumpers generated in a pseudo-random way. This figure, like Fig. 13, also shows perfectly symmetrical contour plots trends with respect to the $e_0 = 0$, axis, with contour plots showing a pseudo-vertical trend for Fig. 14a and a pseudo-horizontal trend for Fig. 14b; therefore, the considerations made previously for Figs. 13a and b on what it means to have pseudo-vertical and pseudo-horizontal contour plots remain valid.

What differentiates Figs. 13 and 14 are the different values of $\beta$ for which they were plotted; these two values were chosen in such a way that when moving from the value of $\beta = 1.05$ to the value of $\beta = 1.20$ there is a point of change in behavior. In fact, comparing Figs. 13a and 14a it is possible to notice how in one case an increase in $\delta_0$ leads to an increase in the response while in the other it leads to a reduction of the response; instead, comparing Figs. 13b and 14b it is possible to notice how the eccentricity of the response is not influenced by the point of change in behavior.

The relationships between input and output quantities just shown, although they are related to a certain response quantity (contact force) and to certain values of $\beta$, appear to also be representative of the other response quantities provided that for the totality of the bumper configurations generated in a pseudo-random way the collision occurs.

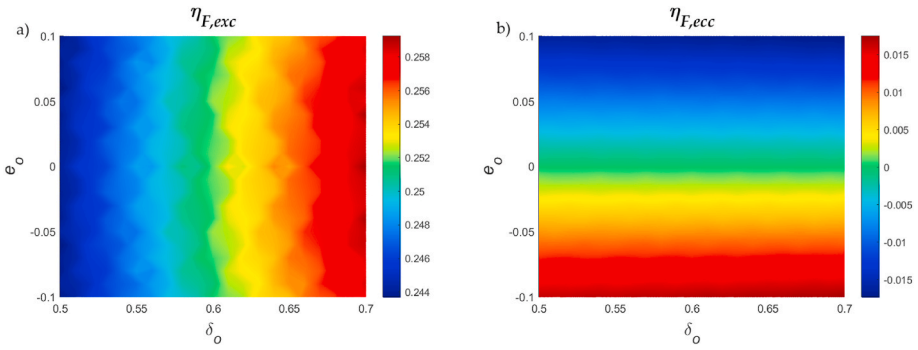


**Fig. 13.** Relationship between the input and output parameters obtained for a value of $\xi = 0.1$, for values of $\lambda = 0.45$ and $\gamma = 2.26$ that derive from the optimal design relating to the reference configurations ($\delta_0 = 0.6$ and $e_0 = 0$). In a) and b) the trend of the excursion and eccentricity of the contact force of the bumpers is reported as $\delta_0$ ed $e_0$ vary for a value of $\beta = 1.05$.

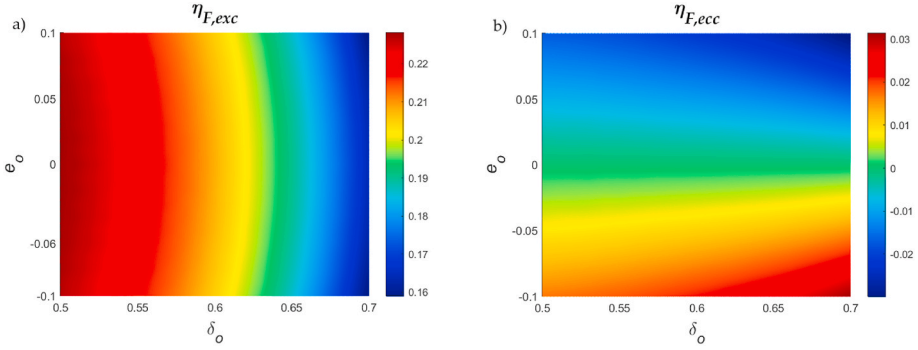


**Fig. 14.** Relationship between the input and output parameters obtained for a value of $\xi = 0.1$, for values of $\lambda = 0.45$ and which derive from the optimal design relating to the reference configurations ($\delta_0 = 0.6$ and $e_0 = 0$). In a) and b) the trend of the excursion and eccentricity of the contact force of the bumpers is reported as $\delta_0$ and $e_0$ vary for a value of $\beta = 1.20$.

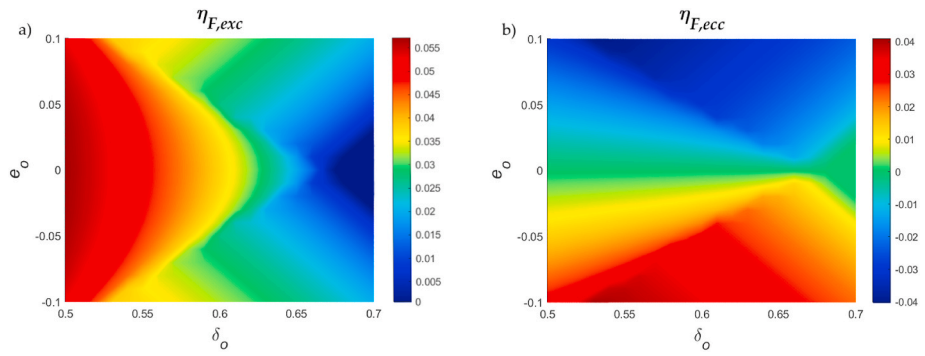


**Fig. 15.** Relationship between the input and output parameters obtained for a value of $\xi = 0.1$, for values of $\lambda = 0.45$ and $\gamma = 2.26$ that derive from the optimal design relating to the reference configurations ($\delta_0 = 0.6$ and $e_0 = 0$). In a) and b) the trend of the excursion and eccentricity of the contact force of the bumpers is reported as $\delta_0$ and $e_0$ vary for a value of $\beta = 0.65$.

Fig. 15 shows the relationship between the parameters $\delta_0$ and $e_0$ and the response quantities excursion and eccentricity of the contact force of the bumpers, for the case which has as reference configuration $\delta_0 = 0.6$ and $e_0 = 0$ and for a value of $\beta = 0.65$. In this case, for bumper configurations that have values of $\delta_0 > 0.68$ and values of $e_0$ between $-0.02$ and 0.02 the collision does not occur; this means that for these configurations the response will always be the same (equal to that which occurs in FF conditions) and this means that the contour plots lose the characteristic of being pseudo horizontal and pseudo vertical.

## 5. Statistical characterization of the nonlinear dynamic response

This section shows how generating bumper configurations in a probabilistic manner leads to responses that also have a probabilistic nature; furthermore, using a statistical test, it is verified whether the distributions of the response quantities are also normal.

### 5.1. Distribution of the output

As was shown in Sect. 4, each response quantity has its own confidence zone characterized by its own length and its own width, the latter which varies as β varies. Therefore, once a response quantity and a value of β have been fixed, the confidence zone assumes a certain width. This means that the response quantity can take on all the results shown in that range, but not all the results will have the same probability of occurring; in fact, just as some bumper configurations are much more probable than others, the same thing happens for the response quantities.

To visualize the probability distributions of the output quantities, histograms are used, just as done for the input quantities.

Fig. 16 shows how the excursion of the relative displacement of the mass is distributed, for the case with the reference configuration $\delta_0 = 0.6$ and $e_0 = 0$, for different values of $\beta$ (1.10, 0.60, 1.30). For each value of $\beta$ both the forward (in blue) and backward (in red) histograms are plotted. As can be seen, these histograms overlap almost perfectly, giving rise to a single purple histogram. This representation allows us to observe how, following an optimal design of $\lambda$ and $\gamma$, the forward and backward responses do not show significant differences even if the gap values deviate from the optimal value.

As can be seen from Fig. 16, although the input distribution always remains the same for each value of $\beta$, the output distribution also varies significantly as $\beta$ varies.

Although the distributions vary as $\beta$ varies, for each distribution if we average all the responses, we observe that this average always tends towards the response of the reference configuration.

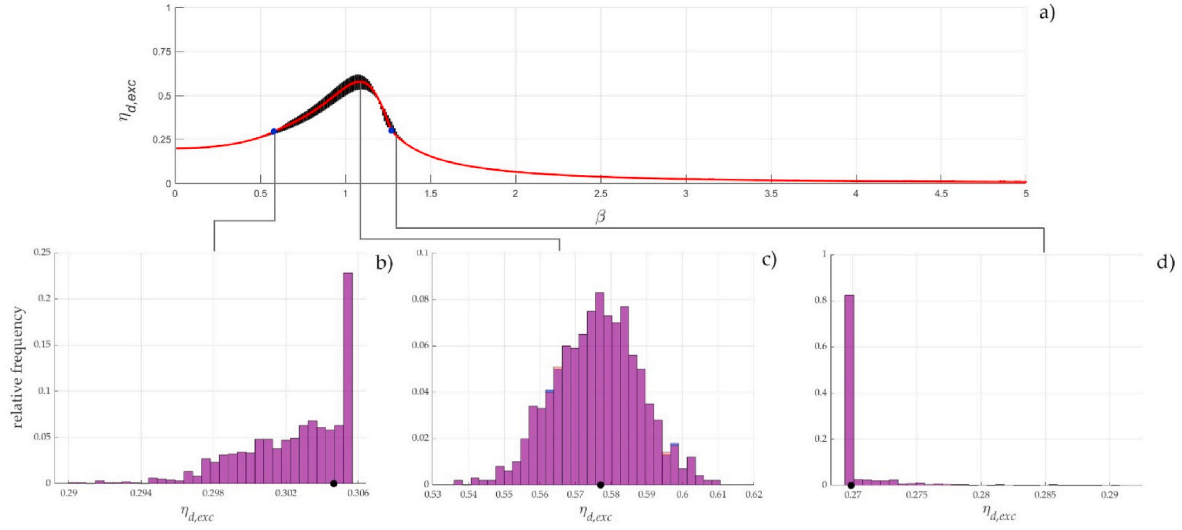


**Fig. 16.** Distribution of the excursion of the relative displacement of the mass obtained for a value of $\xi = 0.1$, for values of $\lambda = 0.45$ and $\gamma = 2.26$ which derive from the optimal design relating to the reference configurations ($\delta_0 = 0.6$ and $e_0 = 0$). In Fig. a) the PRCs of the excursion of the relative displacement of the mass are reported; in b), c) and d) three different histograms plotted for the following values of β 1.10, 0.60 and 1.30 are reported; the histograms in blue represent the forward responses while those in red represent the backward responses; the black dots present in the histograms represent the values assumed by the response quantity for the reference configuration.

For all the excursions of the response quantities relating to the case with reference configuration $\delta_0 = 0.6$ and $e_0 = 0$ it is possible to observe a behavior similar to that reported in Fig. 16: for a range of $\beta$ values located in the vicinity of the resonance the distribution of the response tends to be normal like the input quantities (Fig. 16b), moving away from this range the normal distribution curve tends to shift to one side and most of the response values tend to group into a single bin (as shown in Fig. 16c and d); this grouping process into a single bin will be concluded when the value of $\beta$ is reached for which no collision occurs for all the bumper configurations.

Fig. 17 shows how the eccentricity of the relative displacement of the mass is distributed, for the case with the reference configuration $\delta_0 = 0.6$ and $e_0 = 0$, for different values of $\beta$ (1.10, 0.60, 1.30). For each value of $\beta$ both the forward (in blue) and backward (in red) histograms are plotted. As can also be seen in this case, these histograms overlap almost perfectly, giving rise to a single purple histogram.

Although the distributions vary as $\beta$, varies, for each distribution if we average all the responses, we observe that this average always tends towards the response of the reference configuration.

For all the eccentricities of the response quantities relating to the case with reference configuration $\delta_0 = 0.6$ and $e_0 = 0$ it is possible to observe a behavior similar to that reported in Fig. 17: for a range of $\beta$ values located in the vicinity of the resonance the distribution of the response tends to be of a normal type like the input quantities (Fig. 17b), moving away from this range the values tend to all concentrate in a single bin (the one relating to the response in FF conditions); unlike the distributions of the response excursions, the distributions of the eccentric response quantities always show a rather marked symmetry (symmetry which will be perfect if one follows the hypotheses reported in section 4.3).

Fig. 18 shows how the excursion of the relative displacement of the mass is distributed, for the case with the reference configuration $\delta_0 = 0.06$ and $e_0 = 0$, for different values of $\beta$ (0.01, 1.00, 2.00 and 3.00).

For all the excursions of the response quantities relating to the case with reference configuration $\delta_0 = 0.06$ and $e_0 = 0$ it is possible to observe a behavior similar to that reported in Fig. 18: starting from a value of $\beta$ which tends to zero, the distribution of the response shows a tendency towards normal distribution (as shown in Fig. 18b) and this tendency is maintained for a wide range of $\beta$ values, in particular up to $\beta = 1.45$; for further increases in the $\beta$ value the normal distribution curve first tends to move to one side (as shown in Fig. 18d) and then to the other side (as shown in Fig. 18e) and most of the values will tend to cluster into a single bin.

Fig. 19 shows how the eccentricity of the relative displacement of the mass is distributed, for the case with the reference configuration $\delta_0 = 0.06$ and $e_0 = 0$, for different values of $\beta$ (0.01, 1.00, 3.00).

For all the eccentricities of the response quantities relating to the case with reference configuration $\delta_0 = 0.06$ and $e_0 = 0$ it is possible to observe a behavior similar to that reported in Fig. 19: starting from a value of $\beta$ which tends to zero, the distribution of the response shows a tendency towards a normal distribution (as shown in Fig. 19b) and this tendency is maintained up to a value of $\beta = 2.00$; moving away from this range all the values tend to group into a single bin but the distributions will continue to show a marked symmetry (as shown in Fig. 19d).

As shown for Figs. 16–19, the histograms for the forward (blue) and backward (red) output quantities are approximately equal (purple, as a red and blue overlay). These small differences are attributable to numerical errors and can be eliminated by increasing the number of cycles of the analysis to reach steady-state condition, therefore uncertainties about the gaps do not lead to variations in the response, which is hence unique, even if conditioned by a variation in initial conditions. This can be attributed to good robustness of optimal design of bumpers' characteristics, in contrast to the case of bumpers not designed in accordance with the optimal design [39].

### 5.2. Normality preservation intervals

Through statistical tests, particularly through tests of goodness of fit, we test for which ranges of $\beta$ the distributions of the response quantities can be assumed to be normal.

A statistical test is a rule by which it is decided whether or not to accept a hypothesis formulated on the basis of the sample findings. The hypothesis to be tested is usually denoted by the symbol $H_0$ and called the null hypothesis, if the result of the statistical test is negative (i.e., the null hypothesis cannot be accepted) the rejection of the $H_0$ hypothesis leads to the acceptance of the $H_1$ hypothesis called the alternative hypothesis [54].

The hypothesis to be tested takes the following form:

$$H_0 : f(z) = f_0(z) \quad versus \quad H_1 : f(z) \neq f_0(z) \tag{11}$$

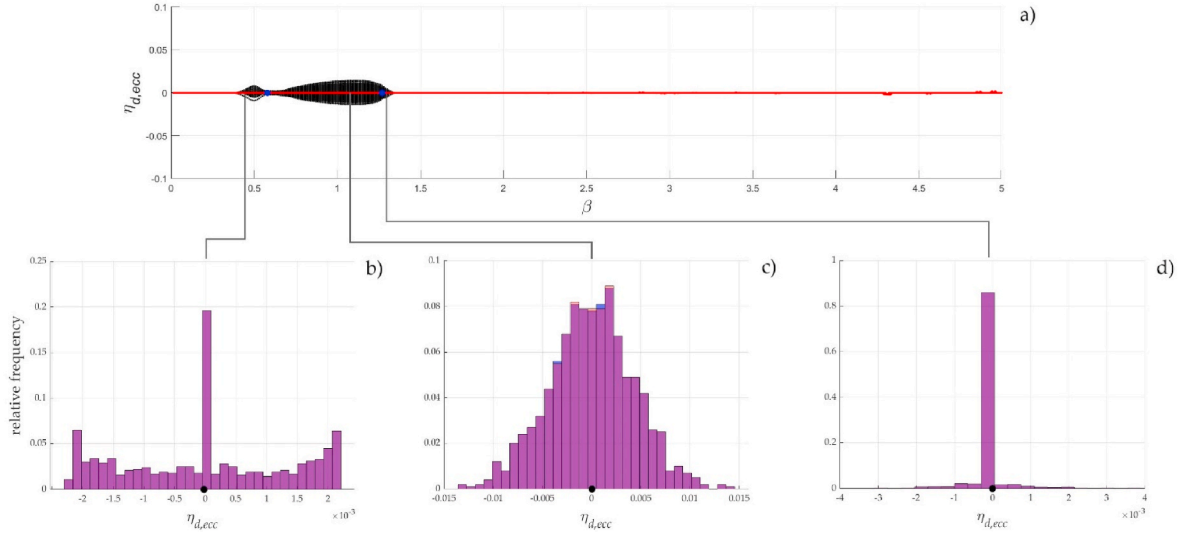


**Fig. 17.** Distribution of the eccentricity of the relative displacement of the mass obtained for a value of $\xi = 0.1$, for values of $\lambda = 0.45$ and $\gamma = 2.26$ which derive from the optimal design relating to the reference configurations ($\delta_0 = 0.6$ and $e_0 = 0$). In Fig. a) the PRCs of the eccentricity of the relative displacement of the mass are reported; in b), c) and d) three different histograms plotted for the following values of β 1.10, 0.60 and 1.30 are reported; the histograms in blue represent the forward responses while those in red represent the backward responses; the black dots present in the histograms represent the values assumed by the response quantity for the reference configuration.

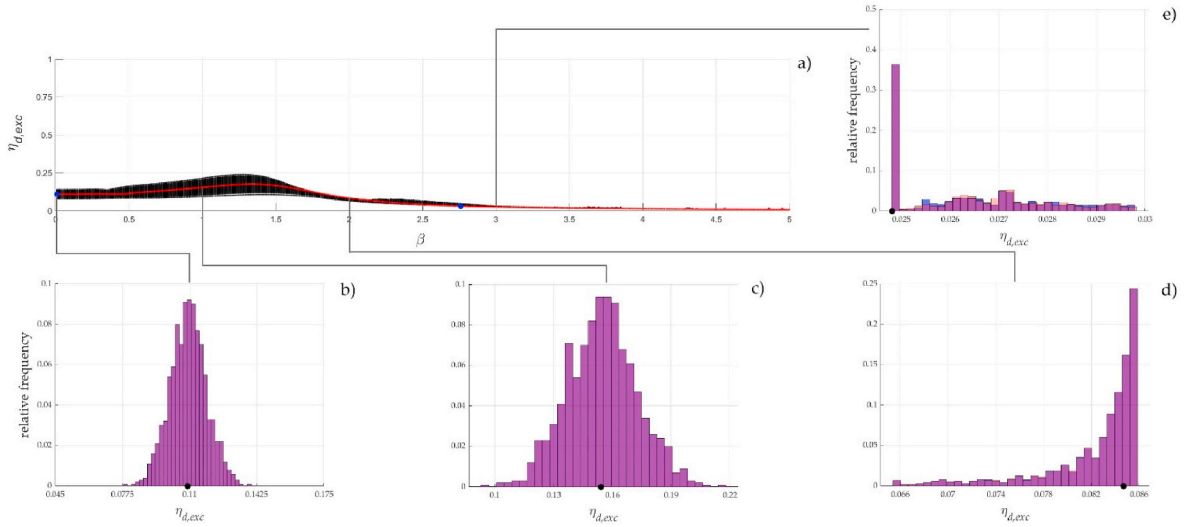


**Fig. 18.** Distribution of the excursion of the relative displacement of the mass obtained for a value of $\xi = 0.1$, for values of $\lambda = 1.14$ and $\gamma = 5.70$ which derive from the optimal design relating to the reference configurations ($\delta_0 = 0.06$ and $e_0 = 0$ In Fig. a) the PRCs of the excursion of the relative displacement of the mass are reported; in b), c), d) and e) four different histograms plotted for the following values of $\beta$ 0.01, 1.00, 2.00 and 3.00 are reported; the histograms in blue represent the forward responses while those in red represent the backward responses; the black dots present in the histograms represent the values assumed by the response quantity for the reference configuration.

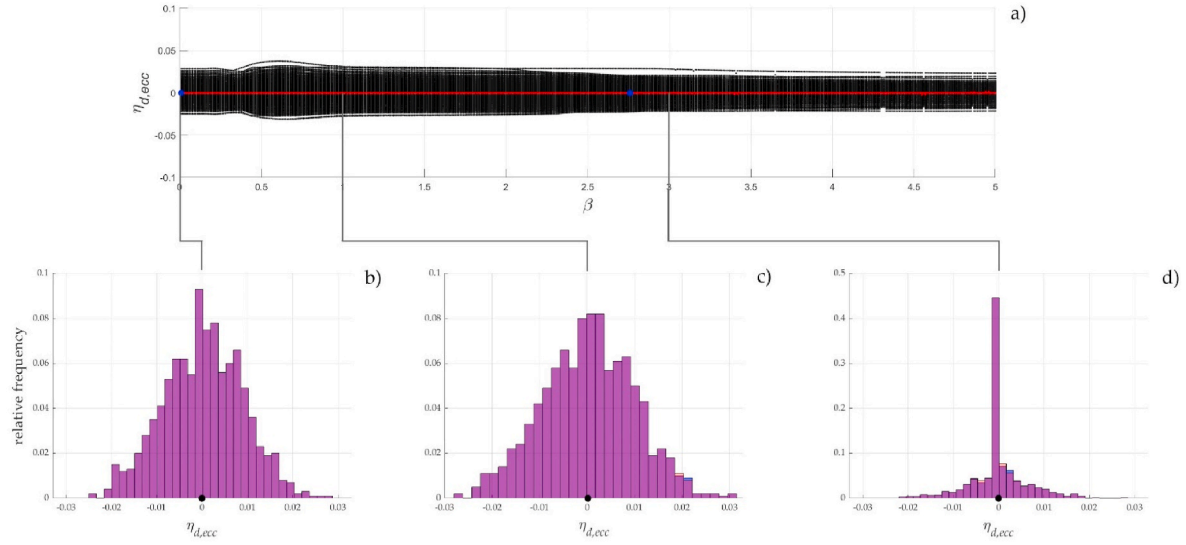


**Fig. 19.** Distribution of the eccentricity of the relative displacement of the mass obtained for a value of $\xi = 0.1$, for values of $\lambda = 1.14$ and $\gamma = 5.70$ which derive from the optimal design relating to the reference configurations ($\delta_0 = 0.06$ and $e_0 = 0$). In a) the PRCs of the eccentricity of the relative displacement of the mass are reported; in b), c) and d) three different histograms plotted for the following values of $\beta$ 0.01, 1.00 and 3.00 are reported; the histograms in blue represent the forward responses while those in red represent the backward responses; the black dots present in the histograms represent the values assumed by the response quantity for the reference configuration.

which consists in evaluating whether the distribution $f(z)$ of the generic random variable z (where z in our case is the value assumed by the generic response quantity) is significantly equal to the theoretical distribution $f_0(z)$.

The theoretical distribution $f_0(z)$ can be completely or only partially specified; in the case in which the hypothesis is completely specified, hypotheses are also made on the values of the parameters that characterize the probability distribution, while in other cases the hypothesis concerns only the type of probability distribution of $f_0(z)$. If, in addition to the type of distribution, hypotheses are also made on the parameters of the distribution, as they are not known, these parameters are calculated starting from the sample of responses observed.

In our case the hypothesis is to verify whether the sample is arranged according to a normal probability distribution and since the parameters of the distribution are not known, further hypotheses are made on the parameters, which are assumed to be like the mean and standard deviation of the sample:

$$\begin{cases} \mu = \dfrac{\sum_i f_i x_i}{n} & (12a) \\ \sigma^2 = \dfrac{\sum_i (x_i - \mu)^2}{n} & (12b) \end{cases} \tag{12}$$

Once these parameters are known, the distribution $f_0(z)$, is known, which in this case is a continuous probability function. To carry out the statistical test it is necessary to pass from the PDF to histograms

consistent with those present in Fig. 16 and to do so it is necessary to carry out as many integrals of the PDF as there are bins present in these histograms. At the end of this operation, we have both the histograms shown in Fig. 16 (which derive from the observed distribution $f(z)$) and histograms that are derived from the assumed normal distribution $f_0(z)$.

The test on the goodness of fit chosen is called the chi-square test and consists of verifying whether the following inequality is satisfied:

$$\chi^2_{k-1} = n\sum_{j=1}^{k}\frac{\left(f_j - \pi_{0j}\right)^2}{\pi_{0j}} \le \chi^2_{k-1,1-\alpha} \tag{13}$$

To the left of the inequality reported in Eq. (13) we have: n = sample size, k = number of bins (histogram rectangles), $f_j$ is the value assumed by the j-th bin of the ''real'' histograms (those in Fig. 16), $\pi_{0j}$ is the value assumed by the j-th bin of the histograms obtained by integrating the hypothesized $f_0(z)$.

To the right of the inequality reported in Eq. (13), given that the test function is distributed as a chi-square variable with a number of degrees of freedom equal to k-1 (or k-q-1 if also the parameters of the distribution have been estimated, where q = number of estimated parameters), we have: $\chi^2_{k-1,1-\alpha}$ the quantile of order $\alpha$ of the chi-square variable with k-1 (k-q-1) parameters; $\alpha$ is known in the literature as the level of significance and is the parameter that allows defining the regions of acceptance and rejection of the hypothesis.

If the hypothesis is not verified, we have the certainty that, for the generic value of $\beta$ and for the generic response quantity, the distribution is not of the normal type (strong rejection of the hypothesis); instead, if the test is verified, the verified hypothesis can be assumed with a significance level $\alpha$ (weak acceptance of the hypothesis). For the purpose of this study this level of acceptance is considered more than sufficient.

Fig. 20 shows the verification of the statistical test carried out for the excursion of the relative displacement of the mass and carried out for each value of $\beta$; in this figure the range of $\beta$ for which the red curve is below the blue curve identifies the range for which the output distribution can be assimilated to a normal distribution, thus identifying the interval of conservation of the normality of the response quantity: range of relative displacement. The normal distributions identified will all have as parameter $\mu$ (average) the response value assumed by the reference configuration for that specific $\beta$. However, as regards the standard deviation (which is an index of dispersion) it does not remain constant for the range of $\beta$ in which the output distribution can be assumed to be normal; this can be immediately observed in Fig. 7 where it is possible to notice how the confidence zone does not always have the same width (therefore the response is not always dispersed in the same way).

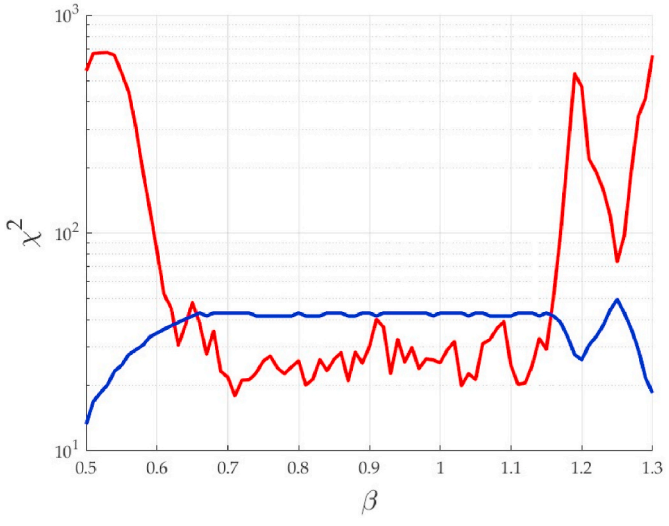


**Fig. 20.** Verification of the chi-square statistical test with a significance level α = 0.01 carried out for the excursion of the relative displacement of the mass ($\eta_{d,max}$), for a system with ξ = 0.1, for values of λ = 0.45 and γ = 2.26 which derive from the optimal design relative to the reference configurations ($\delta_0 = 0.6$ and $e_0 = 0$). The red curve represents the term on the left of the inequality reported in Eq. (13) (the demand), while the blue curve represents the term on the right of the inequality reported in Eq. (13) (the capacity).

For the reference configuration $\delta_0 = 0.6$ and $e_0 = 0$ the normality conservation intervals for the excursions of the response quantities are on average between $0.65 < \beta < 1.15$, while for the eccentricity of the response quantities they are on average between $0.7 < \beta < 1.25$.

For the reference configuration $\delta_0 = 0.06$ and $e_0 = 0$ the normality conservation intervals for the excursions of the response quantities are on average between $0 < \beta < 1.45$, while for the eccentricity of the response quantities they are on average between $0 < \beta < 2.00$.

## 6. Conclusions

In this work, the nonlinear dynamic response of a two-sided vibro-impact single-degree-of-freedom system under harmonic base excitation was studied. Specifically, it was studied by numerical analysis how the uncertainties on the gap values (excursion $\delta_0$ and eccentricity $e_0$), with respect to symmetrical ($e_0 = 0$) and positive ($\delta_0 > 0$) initial gap values, affect the nonlinear dynamic response of the vibro-impact system.

Two cases related to two different reference configurations of optimally designed bumpers [32,41,42] were considered in this study. Compared with the two reference cases, configurations of the bumpers, excursion $\delta_0$ and eccentricity $e_0$ were generated in a pseudo-random way, and by modeling the uncertainty of the gaps through normal probability distributions. The nonlinear dynamic response of the vibro-impact system was evaluated under steady-state conditions.

The results obtained in the two cases considered can be taken as representative of a much larger case series: the first case studied, excursion $\delta_0 = 0.6$ and eccentricity $e_0 = 0$, was taken as representative of all those initial configurations that present $\delta_0 > 0.38$ (which corresponds to the value of $\delta_{0R} = \delta_{0L} = 0.19$, i.e., that case that corresponds to impact occur for $\beta = 0$) and $e_0 = 0$, while the second case, excursion $\delta_0 = 0.06$ and eccentricity $e_0 = 0$, was assumed to be representative of all those reference configurations that present $0 \le \delta_0 \le 0.38$ and $e_0 = 0$ and that can result in configurations with even negative gap values.

From the analyses conducted, the following conclusions can be deduced should the collision occur.

- the presence of an uncertainty in the value of the input data related to the gap (excursion $\delta_0$ and eccentricity $e_0$) is reflected in an uncertainty in the values of the output data, i.e., of the response quantities considered (the absolute accelerations and relative displacements of the mass and the deformations and forces of the bumpers). This leads responses to take values within a certain range, called the confidence zone;
- the confidence zones, for the various response quantities, vary in both length ($\beta$ frequency range) and width (response range). This highlights how each response quantity is differently affected by uncertainties in the gap values;
- for the vibro-impact system with a reference configuration of $\delta_0 = 0.6$ and $e_0 = 0$ (first case), the confidence zones have a significantly smaller length and width than for the vibro-impact system that have a reference configuration of $\delta_0 = 0.06$ and $e_0 = 0$ (second case);
- Comparison between the values of the gap data and the results of the response quantities in terms of excursion $\delta_0$ and of eccentricity $e_0$ showed that the excursions of the response quantities depend almost exclusively on the excursion of the gap ($\delta_0$), while the eccentricities of the response depend almost exclusively on the eccentricity of the gap ($e_0$);
- the confidence zones related to the eccentricity of the response quantities show symmetry; this result is a direct consequence of the

symmetry of the vibro-impact system, which causes that at the same gap excursion ($\delta_0$) two gap eccentricities equal in modulus but opposite in sign lead, respectively, to eccentricities of the response quantities equal in modulus but opposite in sign. Furthermore, it has been observed that a positive gap eccentricity does not always correspond to a response quantities eccentricity of the same sign; such a link between the sign of the gap eccentricity and the sign of the response eccentricity for some response quantities does not remain constant along the length of the confidence zones (as it happens for the relative mass displacement, for the first case, and absolute mass acceleration, for the second case);

- the confidence zones related to the excursion of the response quantities showed, for some values of $\beta$, the presence of some nodal points or zones of change in behavior; that is, points which define ranges of the confidence zones that show responses that, compared with the reference response, are first greater and later less and conversely. These results show how uncertainty about the configuration of bumpers leads to having both ranges of $\beta$ to which correspond response excursion values that are greater than those of the reference, and ranges of $\beta$ to which correspond response excursion values that are smaller;
- it turned out that each value of $\beta$ that falls within the confidence zone is associated with a different probability distribution, although the probability distributions of the gap are always the same. For the two cases analyzed, trends were found for both the excursions and eccentricities of the response quantities that describe how the probability distributions of the output vary as the $\beta$ changes;
- using statistical tests, ranges of $\beta$ were finally identified in which the response quantities retain the same probability distribution as the input, that is, a normal distribution. In these ranges, the probability distribution of the response quantities has a mean value tending to the value assumed by the reference response and a standard deviation varying with $\beta$. The ranges showing a response with normal distribution are larger for the first reference case ($\delta_0 = 0.06$ and $e_0 = 0$) than for the second reference case ($\delta_0 = 0.6$ and $e_0 = 0$).

A possible future development of the work is related to considering the role of uncertainties in the stiffness and damping parameters of bumpers.

Another future development is to consider techniques for controlling uncertainties to direct them toward optimizing the response.

## CRediT authorship contribution statement

**Domenico Pagano:** Writing – original draft, Software, Methodology, Investigation, Data curation, Conceptualization. **Giuseppe Perna:** Writing – original draft, Software, Methodology, Investigation, Data curation, Conceptualization. **Maurizio De Angelis:** Writing – review & editing, Writing – original draft, Validation, Supervision, Project administration, Methodology, Investigation, Funding acquisition, Data curation, Conceptualization. **Ugo Andreaus:** Writing – review & editing, Writing – original draft, Validation, Supervision, Project administration, Methodology, Investigation, Funding acquisition, Data curation, Conceptualization.

## Declaration of competing interest

The Authors wish to confirm that there has been no significant financial support for this work that could have influenced its outcome.

## Data availability

No data was used for the research described in the article.

## Acknowledgments

This work was partially funded by Sapienza University of Rome [grant numbers RM122181679B1216 and RM12117A5DF79E88].

## References

[1] F. Naeim, J.M. Kelly, Design of Seismic Isolated Structures: from Theory to Practice, 1999.
[2] E. Renzi, M. De Angelis, Optimal semi-active control and non-linear dynamic response of variable stiffness structures, J. Vib. Control 11 (10) (Oct. 2005) 1253–1289, https://doi.org/10.1177/1077546305054597.
[3] M. Ismail, J. Rodellar, F. Pozo, Passive and hybrid mitigation of potential near-fault inner pounding of a self-braking seismic isolator, Soil Dynam. Earthq. Eng. 69 (Feb. 2015) 233–250, https://doi.org/10.1016/j.soildyn.2014.10.019.
[4] R.S. Jangid, J.M. Kelly, Base isolation for near-fault motions, Earthq. Eng. Struct. Dynam. 30 (5) (2001) 691–707, https://doi.org/10.1002/eqe.31.
[5] M. Dicleli, S. Buddaram, Equivalent linear analysis of seismic-isolated bridges subjected to near-fault ground motions with forward rupture directivity effect, Eng. Struct. 29 (1) (Jan. 2007) 21–32, https://doi.org/10.1016/j.engstruct.2006.04.004.
[6] M. Basili, M. De Angelis, Optimal passive control of adjacent structures interconnected with nonlinear hysteretic devices, J. Sound Vib. 301 (1–2) (Mar. 2007) 106–125, https://doi.org/10.1016/j.jsv.2006.09.027.
[7] M. Basili, M. De Angelis, A reduced order model for optimal design of 2-mdof adjacent structures connected by hysteretic dampers, J. Sound Vib. 306 (1–2) (Sep. 2007) 297–317, https://doi.org/10.1016/j.jsv.2007.05.012.
[8] V. Crozet, I. Politopoulos, T. Chaudat, Shake table tests of structures subject to pounding, Earthq. Eng. Struct. Dynam. 48 (10) (Aug. 2019) 1156–1173, https://doi.org/10.1002/eqe.3180.
[9] P.C. Polycarpou, P. Komodromos, On poundings of a seismically isolated building with adjacent structures during strong earthquakes, Earthq. Eng. Struct. Dynam. 39 (8) (2010) 933–940, https://doi.org/10.1002/eqe.975.
[10] V. Crozet, I. Politopoulos, M. Yang, J. Martinez, S. Erlicher, Sensitivity analysis of pounding pounding between adjacent structures, Earthq. Eng. Struct. Dynam. 47 (1) (2018) 219–235, https://doi.org/10.1002/eqe.2949i.
[11] S.A. Anagnostopoulos, Pounding of buildings in series during earthquakes, Earthq. Eng. Struct. Dynam. 16 (3) (1988) 443–456, https://doi.org/10.1002/eqe.4290160311.
[12] P. Komodromos, P.C. Polycarpou, L. Papaloizou, M.C. Phocas, Response of seismically isolated buildings considering poundings, Earthq. Eng. Struct. Dynam. 36 (12) (Oct. 2007) 1605–1622, https://doi.org/10.1002/eqe.692.
[13] M. De Angelis, A. Giaralis, F. Petrini, D. Pietrosanti, Optimal tuning and assessment of inertial dampers with grounded inerter for vibration control of seismically excited base-isolated systems, Eng. Struct. 196 (2019) 109250, https://doi.org/10.1016/j.engstruct.2019.05.091.
[14] D. De Domenico, G. Ricciardi, An enhanced base isolation system equipped with optimal tuned mass damper inerter (TMDI), Earthq. Eng. Struct. Dynam. 47 (5) (2018) 1169–1192.
[15] D. De Domenico, G. Ricciardi, Improving the dynamic performance of base-isolated structures via tuned mass damper and inerter devices: a comparative study, Struct. Control Health Monit. 25 (10) (2018) e2234.
[16] D. De Domenico, N. Impollonia, G. Ricciardi, Soil-dependent optimum design of a new passive vibration control system combining seismic base isolation with tuned inerter damper, Soil Dynam. Earthq. Eng. 105 (2018) 37–53.
[17] M.C. Smith, Synthesis of mechanical networks: the inerter, IEEE Trans. Automat. Control 47 (10) (2002) 1648–1662.
[18] D. De Domenico, G. Ricciardi, Optimal design and seismic performance of tuned mass damper inerter (TMDI) for structures with nonlinear base isolation systems, Earthq. Eng. Struct. Dynam. 47 (12) (2018) 2539–2560.
[19] D. Zahedin Labaf, M. De Angelis, M. Basili, Multi-objective optimal design and seismic assessment of an inerter-based hybrid control system for storage tanks, Bull. Earthq. Eng. 21 (3) (Feb. 2023) 1481–1507, https://doi.org/10.1007/s10518-022-01457-1.
[20] P. Deastra, D.J. Wagg, N.D. Sims, R.S. Mills, Experimental shake table validation of damping behaviour in inerter-based dampers, Bull. Earthq. Eng. 21 (3) (2023) 1389–1409.
[21] D. Pietrosanti, M. De Angelis, A. Giaralis, Experimental seismic performance assessment and numerical modelling of nonlinear inerter vibration absorber (IVA)-equipped base isolated structures tested on shaking table, Earthq. Eng. Struct. Dynam. 50 (10) (2021) 2732–2753.
[22] D. Pietrosanti, M. De Angelis, A. Giaralis, Experimental study and numerical modeling of nonlinear dynamic response of SDOF system equipped with tuned mass damper inerter (TMDI) tested on shaking table under harmonic excitation, Int. J. Mech. Sci. 184 (2020) 105762.
[23] P.C. Polycarpou, P. Komodromos, A.C. Polycarpou, A nonlinear impact model for simulating the use of rubber shock absorbers for mitigating the effects of structural pounding during earthquakes, Earthq. Eng. Struct. Dynam. 42 (1) (2013) 81–100, https://doi.org/10.1002/eqe.2194.
[24] S. Yin, G. Wen, J. Ji, H. Xu, Novel two-parameter dynamics of impact oscillators near degenerate grazing points, Int. J. Non Lin. Mech. 120 (Apr. 2020) 103403, https://doi.org/10.1016/J.IJNONLINMEC.2020.103403.

[25] D. Costa, et al., Chaos in impact oscillators not in vain: dynamics of new mass excited oscillator, Nonlinear Dynam. 102 (2) (Oct. 2020) 835–861, https://doi.org/10.1007/s11071-020-05644-0.
[26] M. Wiercigroch, et al., Versatile mass excited impact oscillator, Nonlinear Dynam. 99 (1) (Jan. 2020) 323–339, https://doi.org/10.1007/s11071-019-05368-w.
[27] H. Gritli, S. Belghith, Diversity in the nonlinear dynamic behavior of a one-degree-of-freedom impact mechanical oscillator under OGY-based state-feedback control law: order, chaos and exhibition of the border-collision bifurcation, Mech. Mach. Theor. 124 (Jun. 2018) 1–41, https://doi.org/10.1016/J.MECHMACHTHEORY.2018.02.001.
[28] J. Ing, E. Pavlovskaia, M. Wiercigroch, Dynamics of a nearly symmetrical piecewise linear oscillator close to grazing incidence: modelling and experimental verification, Nonlinear Dynam. 46 (3) (Nov. 2006) 225–238, https://doi.org/10.1007/s11071-006-9045-9.
[29] M. Asme, V.W.T. Sin, M. Wiercigroch experimental study of a symmetrical Plecewlse base-excited oscillator [Online]. Available: http://asmedigitalcollection.asme.org/appliedmechanics/article-pdf/65/3/657/5465593/657_1.pdf, 1998.
[30] G.W. Luo, X.H. Lv, Y.Q. Shi, Vibro-impact dynamics of a two-degree-of freedom periodically-forced system with a clearance: Diversity and parameter matching of periodic-impact motions, Int. J. Non Lin. Mech. 65 (Oct. 2014) 173–195, https://doi.org/10.1016/J.IJNONLINMEC.2014.04.013.
[31] X. Lyu, Q. Gao, G. Luo, Dynamic characteristics of a mechanical impact oscillator with a clearance, Int. J. Mech. Sci. 178 (Jul. 2020) 105605, https://doi.org/10.1016/J.IJMECSCI.2020.105605.
[32] G. Stefani, M. De Angelis, U. Andreaus, The effect of the presence of obstacles on the dynamic response of single-degree-of-freedom systems: study of the scenarios aimed at vibration control, J. Sound Vib. 531 (Aug. 2022), https://doi.org/10.1016/j.jsv.2022.116949.
[33] U. Andreaus, M. De Angelis, Nonlinear dynamic response of a base-excited SDOF oscillator with double-side unilateral constraints, Nonlinear Dynam. 84 (3) (May 2016) 1447–1467, https://doi.org/10.1007/s11071-015-2581-4.
[34] U. Andreaus, P. Baragatti, M. De Angelis, S. Perno, A preliminary experimental study about two-sided impacting SDOF oscillator under harmonic excitation, J. Comput. Nonlinear Dynam. 12 (6) (Nov. 2017), https://doi.org/10.1115/1.4036816.
[35] U. Andreaus, P. Baragatti, M. De Angelis, S. Perno, Shaking table tests and numerical investigation of two-sided damping constraint for end-stop impact protection, Nonlinear Dynam. 90 (4) (Dec. 2017) 2387–2421, https://doi.org/10.1007/s11071-017-3810-9.
[36] U. Andreaus, M. De Angelis, Experimental and numerical dynamic response of a SDOF vibro-impact system with double gaps and bumpers under harmonic excitation, Int J Dyn Control 7 (4) (Dec. 2019) 1278–1292, https://doi.org/10.1007/s40435-019-00532-x.
[37] U. Andreaus, M. De Angelis, Influence of the characteristics of isolation and mitigation devices on the response of single-degree-of-freedom vibro-impact systems with two-sided bumpers and gaps via shaking table tests, Struct. Control Health Monit. 27 (5) (May 2020), https://doi.org/10.1002/stc.2517.
[38] G. Stefani, M. De Angelis, U. Andreaus, Scenarios in the experimental response of a vibro-impact single-degree-of-freedom system and numerical simulations, Nonlinear Dynam. 103 (4) (Mar. 2021) 3465–3488, https://doi.org/10.1007/s11071-020-05791-4.
[39] G. Stefani, M. De Angelis, U. Andreaus, Numerical study on the response scenarios in a vibro-impact single-degree-of-freedom oscillator with two unilateral dissipative and deformable constraints, Commun. Nonlinear Sci. Numer. Simul. 99 (Aug) (2021), https://doi.org/10.1016/j.cnsns.2021.105818.
[40] G. Stefani, M. De Angelis, U. Andreaus, Influence of the gap size on the response of a single-degree-of-freedom vibro-impact system with two-sided constraints: experimental tests and numerical modeling, Int. J. Mech. Sci. 206 (Sep) (2021), https://doi.org/10.1016/j.ijmecsci.2021.106617.
[41] G. Perna, M. De Angelis, U. Andreaus, Numerical steady-state and transient responses of a SDOF system constrained by two optimally designed bumpers, Structures 57 (Nov. 2023), https://doi.org/10.1016/j.istruc.2023.105270.
[42] G. Stefani, M. De Angelis, U. Andreaus, Exploit the study of the scenarios for the control of the response of single-degree-of-freedom systems with bumpers, J. Sound Vib. (Feb. 2024) 118341, https://doi.org/10.1016/j.jsv.2024.118341.
[43] R. Sampaio, C. Soize, On measures of nonlinearity effects for uncertain dynamical systems—application to a vibro-impact system, J. Sound Vib. 303 (3–5) (Jun. 2007) 659–674, https://doi.org/10.1016/J.JSV.2007.01.033.
[44] M. Dimentberg, Z. Hou, M. Noori, Spectral density of a non-linear single-degree-of-freedom system's response to a white-noise random excitation: a unique case of an exact solution, Int. J. Non Lin. Mech. 30 (5) (Sep. 1995) 673–676, https://doi.org/10.1016/0020-7462(95)00013-E.
[45] Q. Feng, H. He, Modeling of the mean Poincaré map on a class of random impact oscillators, Eur. J. Mech. Solid. 22 (2) (Mar. 2003) 267–281, https://doi.org/10.1016/S0997-7538(03)00015-9.
[46] N.S. Namachchivaya, J.H. Park, Stochastic dynamics of impact oscillators, Journal of Applied Mechanics, Transactions ASME 72 (6) (Nov. 2005) 862–870, https://doi.org/10.1115/1.2041660.
[47] H. Rong, X. Wang, W. Xu, T. Fang, Resonant response of a non-linear vibro-impact system to combined deterministic harmonic and random excitations, Int. J. Non Lin. Mech. 45 (5) (Jun. 2010) 474–481, https://doi.org/10.1016/J.IJNONLINMEC.2010.01.005.
[48] M. Xu, Y. Wang, X.L. Jin, Z.L. Huang, T.X. Yu, Random response of vibro-impact systems with inelastic contact, Int. J. Non Lin. Mech. 52 (Jun. 2013) 26–31, https://doi.org/10.1016/J.IJNONLINMEC.2012.12.010.
[49] X. Gu, W. Zhu, A stochastic averaging method for analyzing vibro-impact systems under Gaussian white noise excitations, J. Sound Vib. 333 (9) (Apr. 2014) 2632–2642, https://doi.org/10.1016/J.JSV.2013.12.027.
[50] J. Li, D. Liu, M. Li, Probabilistic response analysis of nonlinear vibro-impact systems with two correlated Gaussian white noises, Int. J. Non Lin. Mech. 151 (May 2023) 104370, https://doi.org/10.1016/J.IJNONLINMEC.2023.104370.
[51] F. Turki, H. Gritli, S. Belghith, An LMI-based design of a robust state-feedback control for the master-slave tracking of an impact mechanical oscillator with double-side rigid constraints and subject to bounded-parametric uncertainty, Commun. Nonlinear Sci. Numer. Simul. 82 (Mar) (2020), https://doi.org/10.1016/j.cnsns.2019.105020.
[52] H. Gritli, Robust master-slave synchronization of chaos in a one-sided 1-DoF impact mechanical oscillator subject to parametric uncertainties and disturbances, Mech. Mach. Theor. 142 (Dec) (2019), https://doi.org/10.1016/j.mechmachtheory.2019.103610.
[53] F. Turki, H. Gritli, S. Belghith, Robust position control of a two-sided 1-dof impacting mechanical oscillator subject to an external persistent disturbance by means of a state-feedback controller, Complexity 2019 (2019), https://doi.org/10.1155/2019/9174284.
[54] G.K. Kanji, 100 Statistical Tests, third ed., SAGE Publications Ltd, London, 2006.